Experimental Study on the Piping Erosion Mechanism of Gap-Graded Soils Under a Supercritical Hydraulic Gradient

Liang Chen
Hohai University
Yu Wan (wy0209@hhu.edu.cn)
Hohai University https://orcid.org/0000-0003-3508-6126
Jian-Jian He
Zhejiang University
Chun-Mu Luo
State Grid Corporation of China
Shu-fa Yan
Hohai University
Xian-Feng He
Yellow River Institute of Hydraulic Research

Manuscript

Keywords: Piping erosion, Supercritical hydraulic gradient, Flow velocity, Fine content, Relative density

Posted Date: February 11th, 2021

DOI: https://doi.org/10.21203/rs.3.rs-176056/v1

Experimental study on the piping erosion mechanism of gap-graded soils under a supercritical hydraulic gradient

Liang Chen[1,2], Yu Wan[1,2 (*)], Jian-Jian He[3,4,5], Chun-Mu Luo[6], Shu-Fa Yan[1,2] and Xian-Feng He[7]

1. Key Laboratory of Geomechanics and Embankment Engineering, Hohai University, Ministry of Education, Nanjing, Jiangsu 210098, China; 2. Geotechnical Research Institute of Hohai University, Nanjing, Jiangsu 210098, China; 3. Key Laboratory of Soft Soils and Geoenvironmental Engineering of Ministry of Education, Zhejiang University, Hangzhou, Zhejiang 310058, China; 4. Institute of Geotechnical Engineering, Zhejiang University, Hangzhou, Zhejiang 310058, China; 5. Center for Hypergravity Experimental and Interdisciplinary Research, Zhejiang University, Hangzhou, Zhejiang 310058, China; 6. State Grid Changzhou City Jintan District Electric Power Supply Company, Changzhou, Jiangsu 213200, China; 7. Yellow River Institute of Hydraulic Research, Zhengzhou, Henan 450003, China.

Corresponding author: Yu Wan (emails: wy0209@hhu.edu.cn)

Abstract:

Seepage-induced piping erosion is observed in many geotechnical structures. This paper studies the piping mechanism of gap-graded soils

during the whole piping erosion failure process under a supercritical hydraulic gradient. We define the supercritical ratio R_i and study the change in the parameters such as the flow velocity, hydraulic conductivity, and fine particle loss with R_i. Under steady flow, a formula for determining the flow velocity state of the sample with R_i according to the fine particle content and relative density of the sample was proposed; during the piping failure process, the influence of R_{imax} on the rate at which the flow velocity and hydraulic conductivity of the sample increase as R_i decreases was greater than that of the initial relative density and the initial fine particle content of the sample. Under unsteady flow, a larger initial relative density corresponds to a smaller amplitude of increase in the average value of the peak flow velocity with increasing R_i. Compared with the test under steady flow, the flow velocity under unsteady flow would experience abrupt changes. The relative position of the trend line L of the flow velocity varying with R_i under unsteady flow and the fixed peak water head height point A under steady flow were related to the relative density of the sample.

Keywords: Piping erosion • Supercritical hydraulic gradient • Flow velocity • Fine content • Relative density

1. Introduction

Internal erosion is a substantial cause of the destruction of geotechnical engineering structures such as filling dams and embankments (Foster et al., 2000; Richards and Reddy, 2007). Piping seepage is a typical form of instability in soil. S.Van. Baars (2009) pointed out in his report that many dam failures were caused by piping. In recent years, an increasing number of piping erosion accidents have occurred worldwide (Brazil,2019; Laos,2018 and China,2015). Therefore, it can be concluded that piping is a problem worthy of sufficient attention and intensive study, and many scholars have conducted relevant research on this topic (Wang et al., 2015; Hu et al., 2020; Zou et al., 2020; Zhang et al., 2020 and Razavi et al., 2020).

Research on the condition of piping occurrence is a popular topic of piping research. There are various factors that affect the occurrence of soil piping, mainly involving four aspects: seepage conditions (such as the water head type, seepage direction, etc.), geometric conditions (such as the soil particle gradation, particle size ratio, etc.), physical conditions (such as the soil compactness, cohesion, etc.), and stress conditions (such as the confining pressure, stress path, etc. (Schuler, 1995;Kenney and Lau, 1985; Wan and Fell, 2008; Fannin and Moffat, 2006; Chang and Zhang, 2011). The critical

hydraulic gradient (CHG) is an important criterion for evaluating the critical condition of piping erosion and depends on the properties of the soil included in the above physical and geometric conditions aspects (Kenney and Lau, 1985; Aberg,1993; Burenkova,1993; Skempton and Brogan, 1994; McDougall et al., 2013). At present, it is the common to study the CHG in terms of the seepage conditions combined with physical and geometric conditions. For example, a formula for calculating the CHG of internal erosion for various grain sizes in sand gravels was established by Mao et al. (2009); Huang et al. (2017) established a theoretical model under two-dimensional seepage flow and showed that the seepage direction angle was positively related to the CHG; Xie et al. (2018) found that CHG increases as the degree of compaction and clay content increases when investigating the failure mechanism of internal erosion at soil-structure interfaces by a homemade device; Yang and Wang (2017) also designed a new apparatus for investigating piping failures and CHG between uniform sands and gap-graded soils and compared the values of CHG measured with uniform sand and gag-graded soil with Terzaghi's theoretical values. However, these research methods have a defect in that they ignore the influence of the stress state of soil on the occurrence of piping. Therefore, researchers have focused on stress condition factors. Luo

et al. (2013) designed a seepage-erosion-stress coupling piping test apparatus; Chang and Zhang (2011) determined the effects of complex stress states on the CHG of internal erosion; Liang et al. (2017,2019) further developed a new device that can simulate piping in the upward flow direction under a complex stress state. They studied the onset of piping erosion under isotropic and anisotropic stress conditions and found that the CHG under the isotropic stress state and the anisotropic stress state were notably different.

Most of the studies focused on the critical conditions for piping erosion occurrence (research on CHG). However, in practice, the water level of rivers will rise rapidly due to heavy rainfall and cause flooding. Piping erosion usually occurs at high flood levels during the flood season, such as in May 2020, floods caused by heavy rain led to dam bursts in America (2020), and in May, a dam in Uzbekistan (2020) also broke due to flooding. A high flood level also means that the hydraulic gradient will exceed the CHG or even increase far beyond the CHG, which we define as the supercritical hydraulic gradient (SCHG). Since piping erosion is a gradual development process with the loss of fine particles, parameters such as the flow velocity, hydraulic conductivity and hydraulic gradient change constantly with the migration and loss of fine particles in the soil, and the parameters

have a certain change rule in time. Therefore, research on the entire development process of piping erosion under the action of steady flow with a fixed supercritical head height has not received much attention. Meanwhile, due to the effects of tides and waves (Li et al., 2020), high flood levels are not always stable, there may be a sudden peak water level, and after a period of time, the water level will drop to the valley water level. The sudden increase in the hydraulic gradient will lead to a nonequilibrium erosion situation (Vandenboer et al., 2019); therefore, research on the piping erosion mechanism under the action of a cyclically unstable supercritical water head has not attracted attention and is worth researching.

In this paper, we will use a homemade apparatus to test the entire development process of piping erosion failure under stable and unstable supercritical water heads and study the changing regularity of the piping parameters, including flow velocity, hydraulic conductivity and loss of fine particles under a SCHG. Simultaneously, we research the effect of the initial relative density and initial fine particle content of soils on these piping parameters.

2. Test materials, apparatus and procedures

2.1 Materials

The soils used in the test were Yangtze Sand. According to the internal stability criteria for soils proposed by Chang and Zhang (2011b), the gap-graded sand specimens were prepared where the fine fraction had a particle size of 0.075–0.25 mm and the coarse particles had a particle size of 2.0-8.0 mm. The sample grading curve is shown in Fig. 1 (FC represents the initial fine particle content).

2.2 Experimental apparatus

The homemade cylindrical tank is shown in Fig. 2(a). The height is 50 cm, and the inner diameter is 140 mm. There are a total of 8 water pressure sensors numbered from 1 to 8 installed on the sidewall from bottom to top. Water flows through the sample from bottom to top. The length of the sample can be adjusted from 250 mm to 400 mm by setting a cushion seat under the water-permeable plate in the buffer area. On the basis of the previous device in Chen Liang's paper (2015), to improve the accuracy of the collected data and the real-time recording of experimental data, we further improved the instrument and developed a data collection system including a water pressure sensor, a flowmeter,

a switching power supply, a signal converter, and an intelligent paperless recorder. The working relationship of each part is shown in Fig. 2(b).

2.3 Test scheme

The development of piping is a process in which fine particles are transported and taken out in the pores of coarse particles, so the content of the fine particles (FC) has a great influence on the development of piping. According to the geometric conditions, Ke and Takahashi (2012) estimated that FC=37% was the ideal state where FC was close to filling the pores between the coarse particles under the condition that the coarse particle part was loose and the fine particle part was dense. Therefore, in this study, we selected specimens with FC=10%, FC=15%, FC=18%, and FC=25%, which represent the different degrees of filling, to conduct experiments.

In addition, the initial relative density Dr, which is defined as:

(1) $$D_r = \frac{e_{max} - e_0}{e_{max} - e_{min}}$$

is a condition that can influence the volumetric strain during piping erosion and has a great effect on the piping mechanism (Zeng, 2016).

Therefore, we selected three groups of samples with FC values of 10, 18, and 25 and three groups of samples with Dr values of 0.3, 0.6,

and 0.8 to conduct the piping test which is shown in Table 1. In this paper, we defined that the smaller hydraulic gradient when fine particles are slightly washed out and the hydraulic gradient at the inflection point of the v-i (v represents velocity; i represents hydraulic gradient) relationship curve is selected as the CHG (Lu, 2005). The calculation formula of the hydraulic gradient in this study is as follows:

$$\Delta h = \frac{(p_3 - p_8)}{\gamma_w} - L \quad (2)$$

$$i = \frac{\Delta h}{L} \quad (3)$$

△h represents the water head loss of the total sample; P_3 and P_8 are the No. 3 and No. 8 pore pressures, respectively; γ_w is the weight of water; and L is the seepage diameter length.

2.4 Procedures

The test steps were performed as follows:

1. The soil samples were dried in an oven at a temperature of 105° C for 24 hours.

2. These fine and coarse particles were completely blended, and the sand was compacted every 2 ~ 3 cm.

3. The water head slowly increased to saturate the entire sample, which lasted for 24 h, and then the test began.

4. The water head was raised from the height of the samples and slowly saturated every 50 mm, which was fixed for 5 minutes, and lifting of the water head was stopped when the rate of flow increased, which could be observed from the flow meter fixed to the water head. During the whole test, the real-time change curves of water pressure sensors No. 1 to No. 8 and the flow meter in the paperless recorder were observed, simultaneously making a record of the test phenomenon. When no fine particles flowed out from the top surface of the sample and the real-time change curve of the water pressure and flow in the paperless recorder became stable, it was determined that the sample was completely destroyed by piping and then the test was terminated.

3. Results and discussion

3.1 Experimental phenomena

Since the experimental phenomena of the FC and Dr groups are similar, Dr0.6 was selected as a typical experimental phenomenon for illustrating the whole process of piping development.

Fig. 3 is the Dr0.6 saturation sample before lifting the upstream water head, and it can be seen that the fine and coarse particles in the sample are evenly distributed.

Fig. 4 shows the stage of lifting the Dr0.6 upstream water head,

where the seepage quantity tended to decrease and the pore pressure tended to stabilize after every lifting water head stage (a). Typical pictures corresponding to points A, B, C, and D were recorded from the top and side of the sample from the cylindrical tank, which are shown in Fig. 4. When the experiment was carried out for 26 minutes (b), the pulsation of the fine particles occurred in two places, and a small amount of fine particles accumulated in one of them. When the experiment continued for 32 minutes (c), there were two pulsations of the fine particles on the side of the sample. After 47 minutes (d) of the test, it was found that there had been fine particle accumulation in three places on the top of the sample. When the test continued for 57 minutes (e), it was found that there had been relatively obvious fine particle accumulation in the direction from 1:00 to 4:00 on the top of the sample.

Fig. 5(a) shows the changes in the pore pressure and the seepage quantity during the whole process of Dr0.6 piping failure. Point E (b) shows the phenomenon of the top surface of the sample when the test was carried out for 193 minutes. It can be seen that there were many fine particles that accumulated on the top surface of the sample, the seepage quantity was continuously rising, and the pore pressure of No. 3~6 decreased obviously. When the test was carried out for 268 minutes

(c), continuous fine particles gushed out during the test, and the coverage area of the fine particles that accumulated on the top surface of the sample further increased. The increase rate of the seepage quantity became slower, and the rate of the pore pressure drop of No. 3~6 also slowed down. When the test was conducted for 575 minutes (d), corresponding to point G, the sample approached complete piping failure, and the test continued until 695 minutes (e). Tt could be seen that no fine particles were flushed out from the top surface of the sample, and complete piping failure occurred. Meanwhile, compared with Fig. 4, two obvious piping outlets appeared on the top surface (e), and two obvious piping gushing channels appeared on the sidewall of the sample (f).

3.2 Analysis of the piping test results

3.2.1 Flow velocity

The variation in the velocity with time of group FC and Dr during the whole piping development is shown in Fig. 6. Table 2 shows the SCHG i_{scr} when the water head was fixed after the last head lift, hydraulic gradient i_f when complete piping failure occurred and CHG of the sample. We define the supercritical ratio as $R_i=i_s/i_{cr}$ (i_s represents the SCHG) and $R_{imax}= i_{scr}/i_{cr}$ because i_{scr} is the maximum SCHG of the whole

process of piping erosion. The whole process of the piping erosion test consisted of the upstream water head lifting stage and the piping failure stage after the upstream water head was fixed. In the piping failure stage, according to Chen et al. (2020), the solid point M_n (n=1~5) was the critical point where the flow velocity started to increase; similarly, the solid points N_n (n=1~6) and P_n (n=1~6) represented the critical points at which the flow velocity started to become stable and decrease, respectively. Consequently, M_n~ N_n demonstrated that the flow velocity showed an increasing state, N_n~ P_n demonstrated that the flow velocity showed a stable state, and the flow velocity after point P_n showed a decreasing state.

3.2.1.1 Upstream water head lifting stage

Theoretically speaking, when the upstream water head height exceeds the critical head height, the flow velocity should increase with the elevation of the head height. In actual experiments, it was found that with the increase in the head height, the flow velocity did not increase completely over time and might also show a stable or decreasing state. To further study the effect of different SCHGs on the change in the state of the flow velocity over time before the piping erosion failure stage, combined with R_{imax} shown in Table 3, we selected R_{imax} = 1.0, 1.3,

1.6, 1.8, 2.1, 2.5, and 2.8 for each group of samples to conduct the piping test and maintain 90 min at each R_{imax} (it can be seen from Fig. 6 that the upstream water head lifting stage of each group of samples lasted no more than 90 min).

The test phenomena of each group of samples were similar. Therefore, we selected the typical Dr0.6 group (Fig. 7) to analyze and determine that the flow velocity decreased over time when R_{imax} =1.0, 1.3, and 1.6. When R_{imax}=1.8, 2.1, and 2.5, the flow velocity remained stable over time, and it increased over time when R_{imax}=2.8. Therefore, the state of the change in the flow velocity over time during the process of piping is represented as follows: decreasing state, stable state, and increasing state. Consequently, to further study the influence of the initial fine particle content and the initial relative density on the change in the flow velocity over time under the action of various SCHGs, we obtained the distribution of the change state of the flow velocity of each group of samples under each level of the SCHG in the form of points, as shown in Fig. 8.

In Fig. 8, "Area A" is the distribution area where the flow velocity is in a decreasing state, and "Area B" is the distribution area where the flow velocity is in a stable state and increasing state. On the whole, the distribution of the three states of the flow velocity with

the increase in the hydraulic gradient is the decreasing state, stable state and increasing state successively, regardless of how the initial fine particle content or initial relative density of the samples changed. The stable state is a transitional phase between the decreasing state and the increasing state, and its distribution area is small.

In Fig. 8(a), the area where the flow velocity decreased was more to the upper left, that is, the larger the fine particle content of the sample was, the larger the SCHG corresponding to the stable state of the flow velocity. In addition, "Area A and Area B" shifted to the direction of the increase in the hydraulic gradient; in Fig. 8 (b), the flow velocity decreasing state was also more distributed in the upper left, that is, with the increase in the relative density of the sample, the SCHG corresponding to the stable state also increased.

The flow velocity gradually decreased over time because of the fine particles inside the sample blocking the pores when they moved, which resulted in a decrease in the permeability of the sample. Since there was no loss of fine particles in the process of blocking the pores with fine particles, the content of the fine particles and relative density of the sample did not change, but the water head loss in the length direction of the sample's seepage diameter increased due to pore

blockage, so the hydraulic gradient increased. Therefore, with the gradual increase in the amount of fine particles inside the sample to block the pores, the flow velocity gradually decreased. The movement path of the flow velocity state in the test moved from "Area A" to the right, similar to "Point P" and "Point M" shown in Fig. 8.

The flow velocity gradually increased over time because the fine particles inside the sample were washed away from the pores, resulting in greater permeability of the sample. Due to the loss of fine particles, the fine particle content and relative density of the sample gradually decreased, and the water head loss in the length direction of the sample's seepage diameter also decreased, so the hydraulic gradient decreased. Therefore, with the gradual increase in the loss of fine particles inside the sample, the flow velocity increased accordingly. The direction of movement of the flow velocity state in the test was similar to "Point Q" and "Point N" shown in Fig. 8.

To further study the relationship between the state of the flow velocity and R_i, the abscissa in Fig. 8 is replaced with R_i and the distribution diagram of the flow velocity state is drawn, as shown in Fig. 9.

In Fig. 9, the distribution of the three flow velocity states on R_i and the movement path of the points were the same as those in Fig.

8. The distribution law of the stable state of the flow velocity in Fig. 9 was more obvious than that in Fig. 8, as shown in the area between the solid line and the dotted line. It can be seen that with the increase in the fine particle content of the sample, the hydraulic gradient range corresponding to the stable state of the flow velocity gradually became larger; with the increase in the relative density of the sample, the hydraulic gradient range corresponding to the stable state of the flow velocity gradually became larger.

The dividing line of "Area A and Area B" in Fig. 9 was basically a straight line. Under the condition that the ratio of the sample is the same or close to that in this paper, the flow velocity state of the sample under the action of a certain SCHG can be roughly obtained in terms of the fine particle content and density of the sample, respectively, as follows:

In terms of the fine particle content of the sample:

(4) when $R_i < \frac{FC+191}{88}$, the flow velocity was in a decreasing state;

(5) when $R_i \geq \frac{FC+191}{88}$, the flow velocity was in a stable state or increasing state;

In terms of the relative density of the sample:

(6) when $R_i < \frac{D_r+11}{4.889}$, the flow velocity was in a decreasing state;

(7) when $R_i \geq \frac{D_r+11}{4.889}$, the flow velocity was in a stable state or

increasing state;

3.2.1.2 Piping erosion failure stage

Based on Fig. 9, we further plot the change path of the flow velocity state of the whole process of piping erosion, as shown in Fig. 10. Take group Dr0.3 as an example (Fig. 10(a)). Section O~A corresponded to the upstream water head lifting stage and then the water head at point A was fixed, the hydraulic gradient of the sample gradually decreased, and finally, complete piping failure occurred at point D. Point D was located at the junction of the steady state and the descending state of the flow velocity. Combined with Fig. 6, it can be concluded that when R_{imax} =2.38 (FC18), the flow velocity then went through two stages: the stable stage and then the decreasing stage; when R_{imax}＞3 (other 5 groups), the flow velocity then went through three stages: the increasing stage, then the stabilize stage and finally the decreasing stage. Fig. 6(a) shows that the FC25 group did not experience a significant change in the flow velocity until 80 minutes because the fine particle content was too high, which caused the fine particles to block the pores during the early process of raising the water head. When the water head was raised to a height of 3.1, the larger water flow force suddenly flushed away the fine particles,

causing the flow velocity to rapidly increase. Fig. 6(b) shows that point B is the sudden change point of the flow velocity in the Dr0.8 group because during the loss of fine particles, the migration of the fine particles caused the pores to clog again until they were flushed out, resulting in an instantaneous increase in the flow velocity. Therefore, the migration of the particles under the SCHG may also experience the movement-blocking-flushing process, similar to that under the CHG.

Since the hydraulic gradient in the whole process of piping failure after fixing the water head is SCHG, to further study the effect of the SCHG on the flow velocity in the whole process of piping failure, we plot the variation of the flow velocity with R_i, which is shown in Fig. 11.

When fixing the upstream water head, the value of R_i at this time was the maximum, and it can be applicable to both the Dr and FC groups that the greater the value of R_{imax}, the greater the corresponding flow velocity would be when complete piping failure occurred.

The dashed line Ln in the increasing stage of the flow velocity is an approximate slope fitting straight line. It can be seen from Fig. 11(a) that the smaller the initial relative density is, the larger the value of K_{Ln}, which represents the rate of increase of the flow velocity

as R_i decreases. In Fig. 11(b), although the fine particle content of FC10 is smaller than that of FC25, because R_{imax} of FC25 is much larger than that of FC10, which represents the much larger seepage force acting on the sample, the corresponding rate of the increase in the flow velocity is $K_{L4} < K_{L5}$. Combined with Table 3, it can be concluded that when R_{imax} of the different sample are close, the rate of increase of the flow velocity as Ri decreases is related to the relative density of the sample. The smaller the relative density, the greater the rate of increase of the flow velocity. When R_{imax} of the different sample vary greatly, the rate of increase of the flow velocity with the decrease in the value of R_i is related to R_{imax}. The greater R_{imax} is, the greater the rate of increase in the flow velocity.

3.2.2 Hydraulic conductivity

The variation in the hydraulic conductivity with time during the whole piping development is shown in Fig. 12. The hydraulic conductivity went through three stages: the upstream water head lifting stage, increasing stage, and stabilizing stage. During the stage of upstream water head lifting, the change in the hydraulic conductivity is more complicated. During the increasing stages, the increasing rate of the hydraulic conductivity of the three groups of the Dr group (Fig.

12 (a)) were almost equal, and Point K in Fig. 12(a) demonstrates the rapid increase in the hydraulic conductivity of Dr0.8 because the fine particles that clogged the pores were instantly washed away. In Fig. 12(b), FC10 and FC25 had approximately the same rate of increase in hydraulic conductivity and were both larger than that of FC18.

To further study the effect of the SCHG on the hydraulic conductivity during the process of piping development after fixing the upstream water head, the variation in the hydraulic conductivity with R_i is plotted, which is shown in Fig. 13.

On~An (n=1~6) is the upstream water head lifting stage, and the hydraulic conductivity was basically stable with increasing R_i.

An~Bn is the increasing stage. Fig. 13 (a) shows that $K_{L3}>K_{L1}>K_{L2}$. In Fig. 14 (b), $K_{L6}>K_{L4}>K_{L5}$. Combined with Table 3, it can be concluded that the rate of increase of the hydraulic conductivity with the decrease in the value of R_i is related to $R_{imax,}$ which had a greater impact on the hydraulic conductivity than the initial relative density and initial fine particle content. The greater the value of R_{imax} is, the greater the rate of increase of the hydraulic conductivity.

3.2.3 Loss of fine particles

The loss of fine particles is the direct cause of the development

and destruction of piping. Due to the continuous loss of fine particles during the failure of piping, the pores inside the sample will increase, which can cause the permeability and flow velocity of the sample to increase. To intuitively reveal the change rule of the fine particle loss amount, three sets of samples of the Dr group with the same initial fine particle content were selected to plot the variation in the fine particle loss amount corresponding to each stage of the whole piping development (Fig. 14).

In the whole process of piping failure (Fig. 14), the fine particle loss during the upstream water head lifting was very small, almost zero; the increase stage of the flow velocity was the main stage of fine particle loss, accounting for almost 50% of the total fine particle loss; the amount of fine particle loss during the stabilization stage of the flow velocity was greatly reduced; the amount of fine particles lost during the period of decreasing flow velocity increased again (because the duration of the velocity stabilization stage was much less than that of the velocity increasing stage and decreasing stage); after the sample was completely destroyed, the amount of fine particles that were lost was very small.

It is known from the development process of the Dr group (Fig. 6(a)) that the duration of the flow velocity stabilization stage is

much less than half of the duration of the flow velocity decreasing stage. Therefore, although the fine particle loss in the flow velocity decreasing stage was greater than that in the flow velocity stabilization stage, the loss rate of fine particles in the decreasing stage of the flow velocity is less than that in the stabilization stage. This is because there are many fine particles inside the sample that block the pores during the decreasing stage of flow velocity, so the rate of fine particle loss is reduced. The loss of fine particles in the stage of upstream water head lifting is lower because of the shorter duration of the sample under the SCHG; the loss of fine particles in the stage of complete destruction of the sample is lower because the internal piping channel of the sample is completely formed. At this time, the height of the upstream water head is constant, and the permeability of the sample tends to be stable, so the loss of the fine particles is very small.

The order of the mass loss of the fine particles in the three sets of the Dr group during the flow velocity increasing stage was A2> A3> A1. The largest amount of loss of fine particles in Dr0.6 was due to the largest value of R_{imax}; although the value of R_{imax} of Dr0.3 was greater than that of Dr0.8, the relative density of Dr0.3 was much lower than that of Dr0.8. Therefore, the amount of the loss of fine particles was

the smallest. It can be seen that when the relative densities of the samples were the same, the larger the value of R_{imax} was, the greater the amount of loss of fine particles in the increasing stage of the flow velocity; when the values of R_{imax} are the same, the larger the relative density of the sample was, the greater the amount of fine particles lost during the increasing stage of flow velocity. The amount of loss of fine particles of the three sets of samples in the flow velocity stabilization stage was exactly the opposite of the flow velocity increasing phase, and the order was B1> B3> B2. It can be seen that the larger the test value of R_{imax} was, the smaller the loss of fine particles in the stage of the steady flow velocity. The amount of loss of fine particles in the decreasing stage of the flow velocity was C3> C2> C1, indicating that the greater the relative density of the sample was, the greater the amount of loss of fine particles in the decreasing stage of the flow velocity.

3.3 Piping erosion test under the action of unsteady flow

To further study the piping erosion mechanism under unsteady flow, since the critical hydraulic gradient of each group of samples has been determined in Table 3, we chose to set 6 groups of SCHGs with different multiples from low to high (R_i=1.5,2.0,2.5,3.0,3.5,4.0).

After the start of the test, the upstream water head was raised from the height when the sample was saturated. We reciprocated lifting and lowering the water head according to the simplified unsteady circulating water head model determined in section 3.3.1 and repeated it three times for the height of each R_i in order from low to high.

3.3.1 Establishment of the unsteady water head model

To simulate the unsteady water head situation in an actual water conservancy project, the flood peak process line calculated based on the 1994 maximum flood year of the Beijiang River levee (Mao et al. 2005;2005;2004) is selected as the prototype of the unsteady water head model in this paper. The experimental unsteady head model is simplified and established according to the following process.

The value of 12.33 m (Liang XQ, 1994) was taken as the indoor test peak water level 9 m (Liang XQ, 1994) was taken as the warning water level, and the approximate sine curve of the unsteady head above the warning level was converted into an equivalent stable average water head. As shown in Fig. 15(a), SA+SB+SC+SD=SB+SE+SF. The flood peak water level after equivalent transformation lasted for 6 days, and the entire flood peak fluctuation cycle period was T=11 days, which is shown in the simplified flood peak process line in Figure

15(b).

According to the similarity principle (Zhang WJ,2013), it is necessary to make the indoor model test and the real working condition meet the mechanical similarity and use the results of the indoor model test to predict the prototype working condition. We found that Coriolis' law (Mao CX,2013), which is suitable for both the seepage theorem and compressibility, is suitable for estimating the piping test model. The model scales used in this test are as follows:

(8) Length scale:$\lambda_L = \frac{L_y}{L_m}$

(9) Time scale:$\lambda_t = \frac{t_y}{t_m}$

(10) Geometric scale:$\lambda_t = \lambda_L$

λ represents the model scales, the subscripts of λ represent the physical quantity, y represents the physical quantity of the prototype, m represents the physical quantity of the model, L represents the length, h represents the height, and t represents the time.

Taking a typical place where piping occurs for the Beijiang River levee as an example, the test model is calculated as follows: the distance between the piping place and Beijiang is 100 m, which can be seen as the length of the seepage diameter of the piping, and the length of the seepage diameter designed by the test model is 250 mm.

The simplified entire flood peak fluctuation cycle is Ty = 11 days. According to (1), (2), and (3), the entire flood peak fluctuation cycle of the test model can be calculated as shown in Table 3.

3.3.2 Analysis of the flow velocity

The curves according to the relationship between the velocity and time are plotted as shown in Figure 16.

First, in terms of 6 different SCHGs (R_i), regardless of which group of samples was selected (except group FC25), the flow velocity would go through three stages of decreasing, stabilizing, and increasing in the whole test process from R_i=1.5 to 4 successively. The water head of the FC25 group only increased to the height of R_i=3.5 because of the excessive large amount of fine particles, so when it was raised to the first five heights of R_i, the fine particles were blocked in the pores. There was no obvious phenomenon, and then when raised to the height of R_i=4, the excessive high peak water head height caused the flow velocity to be too large and washed away the fine particles, resulting in extremely poor overall experimental results. Similar to steady flows (section 3.2), it can also be determined that the sample experienced piping erosion failure when the flow velocity was in the increasing state. Compared with the piping erosion test

under steady flows, we found that the value of R_i of the occurrence of piping erosion failure of each group of samples under the action of flood peak unsteady flow was smaller than that under the action of steady flow, which was the same as Chen Liang's article (Chen et al. 2013).

Second, in terms of the three cycles under each water head height corresponding to R_i, when the flow velocity went through a decreasing state, the initial peak flow velocity of the second head cycle was larger than the final peak flow velocity of the first head cycle, and the initial peak flow velocity of the third head cycle was larger than the final peak flow velocity for the second cycle. Meanwhile, under the same cycle level, the mutations between the flow velocity at the end point of the previous cycle and the starting point of the next cycle were related to the degree of decrease in the flow velocity during the entire cycle. The larger the change in velocity was, the greater the mutations in the velocity of the two adjacent cycles at the end point and the starting point. Similarly, the change in the velocity was smaller, and the continuity of the velocity of the two adjacent cycles at the end and starting point was better. This is because if the flow velocity was decreasing, it meant that there were cases where fine particles migrated inside the sample, resulting in

blocked pores, and then water flow opened the pores; the fine particles inside the sample were unstable. At this time, if the water head height suddenly dropped or lifted, due to the impact of the seepage force on the sample, some fine particles that were clogged in the pores were flushed away, so the flow velocity was discontinuous. In addition, in Figure 16(b), the flow velocity in the first cycle of the water head height corresponding to R_i=4 of group Dr0.3 increased, but when the water head was raised to the second cycle, the flow velocity was still decreasing first and increasing again; the junction of cycle 2 and cycle 3 of the water height corresponding to R_i=4 of figure (d) and (f) experienced similar situations. Due to the cyclic rise and fall under unsteady flow, the flow velocity was relatively unstable in the short time after the water head was raised to the peak height.

From the analysis of Figure 16, we can find that the change rate of the peak initial flow rate and the peak end flow rate at the same cycle of the same level of SCHG is not very large, so we averaged the flow velocity and the hydraulic gradient under each cycle of each R_i to further analyze the relationship between the flow velocity and R_i.

It can be seen from Fig. 17(a) that $K_{L1}>K_{L2}>K_{L3}$ (L represents the trend line that flow velocity varies with Ri) and that the greater the initial content of fine particles is, the smaller the amplitude of

increase in flow velocity with increasing R_i. From Fig. 17(b), we can see that $K_{L4}>K_{L5}>K_{L6}$ and it can be determined that the larger the initial relative density is, the smaller the amplitude of increase in the flow velocity with the increase in R_i.

3.4 Comparison: under steady flow and unsteady flow

Fig. 18 is plotted to compare the flow velocity varying with R_i under the action of unsteady flow and steady flow (W in Fig. 18 represents the test under steady flow and F in Fig. 18 represents the test under unsteady flow).

It can be seen from Figure 18 (d), (e) and (f) that the relative position of the trend line L of the flow velocity varying with R_i under the unsteady flow test and the fixed peak water head height point A under the steady flow test were related to the relative density of the sample. When the relative density of the sample gradually increased, the flow rate change trend line L gradually moved from the upper left side to the lower right side of point A.

However, in Figure 18 (b)(f), it can be seen that the flow velocity under steady flow (point A) was higher than that under unsteady flow (point B) when the water head heights of the corresponding R_i values were nearly equal. This experimental phenomenon was due to the upstream

water head lifting and falling rate of the unsteady flow piping test being greater than that of the steady flow piping test. If the fine particle content of the sample was higher or the degree of relative density was higher, when the upstream water head height was suddenly raised, a large number of fine particles inside the sample began to migrate, causing the phenomenon of fine particles blocking the pores, so the flow velocity was less than that under steady flow.

Conclusions

Based on the homemade test device, a series of laboratory tests were conducted to study the piping erosion mechanism of gap-graded soils under a supercritical hydraulic gradient. We defined the supercritical ratio R_i and studied the law of the flow velocity and other parameters varying with R_i. The following main conclusions were drawn as follows:

1. Through the 90-minute steady water head piping erosion test under different supercritical water head heights, the change in the flow velocity exhibited the following sequence: decreasing state, stable state, and increasing state. According to the distribution of the flow velocity state with the change in R_i, a formula for determining the flow velocity state of the sample with R_i according to the fine

particle content and relative density of the sample was proposed.

2. During the piping erosion failure process after the upstream water head was fixed, the change in the flow velocity with time successively went through an increasing stage, stable stage and decreasing stage, and the influence of R_{imax} on the rate at which the flow velocity of the sample increased as R_i decreased was greater than that of the initial relative density and the initial fine particle content of the sample. The change in the hydraulic conductivity with time successively went through an increasing stage and stable stage. The rate of increase of the hydraulic conductivity with the decrease in R_i was related to $R_{imax,}$ which had a greater impact on hydraulic conductivity than the effect of the initial relative density and initial fine particle content of the sample on the hydraulic conductivity.

3. During the piping erosion failure process, the increasing flow velocity stage was the main stage of fine particle loss, accounting for 50% of the total fine particle loss; although the cumulative loss of fine particles in the flow velocity decreasing stage was greater than that in the flow velocity stable stage, the rate of fine particle loss in the flow velocity decreasing stage was less than that in the flow velocity stable stage. When the relative

densities of the samples were the same, the greater the value of R_i was, the greater the loss of fine particles during the flow velocity increasing stage; when the values of R_i were the same, the greater the relative density of the sample was, the greater the loss of fine particles during the flow velocity increasing stage.

4. During the piping erosion test under the action of unsteady flow, under the supercritical water head height corresponding to the same R_i values, the peak flow velocity between adjacent water head cycles was discontinuous, and the sudden change in the peak flow velocity depended on the amplitude of the increase or decrease in the flow velocity at this water head height. Through the relationship between the average value of the peak flow velocity and R_i, it could also be determined that the larger the initial relative density was, the smaller the amplitude of increase in flow velocity with increasing R_i.

5. Compared with the piping erosion test under steady flow, at the same supercritical water head height corresponding to R_i, the flow velocity under unsteady flow was not always greater than the flow velocity under steady flow. For samples with more fine particles or a larger relative density, the sudden increase in the upstream water head would cause the migration of a large number of fine particles

and block the pores, which would lead to a lower flow velocity than that under steady flow.

Acknowledgements

The authors gratefully acknowledge for the financial support comes from the National Natural Science Foundation of China (Grant No. 51778210) and Open Project Funded by the Engineering And Technical Research Center for Dike Safety and Disease Control of the Ministry of Water Resources (Grant No. DFZX202004).

Data Availability Statement

Some or all data, models, or code that support the findings of this study are available from the corresponding author upon reasonable request.

References

Aberg, B. 1993. Washout of grains from filtered sand and gravel materials. Journal of Geotechnical Engineering, doi:10.1061/(ASCE)0733-9410 (1993)119:1(36).

America (2020)https://m.sohu.com/a/398193966_164659/?pvid=000115_3w_a

Baars, S.V. 2009. The causes and mechanisms of historical dike failures

in the Netherlands. Official Publication of the European Water Association (EWA).

Brazil (2019)http://news.sina.com.cn/o/2019-01-26/doc-ihqfskcp0519310.shtml

Burenkova, V.V. 1993. Assessment of suffusion in non-cohesive and graded soils. In: Brauns, J., Heibaum, M. (Eds.), U.S. Filters in Geotechnical and Hydraulic Engineering. Balkema, Rotterdam, the Netherlands, pp. 357–360.

Chang, D.S. and Zhang, L.M. 2011. Internal stability criteria for soils. Rock and Soil Mechanics, 32(S1):253-259.

Chang, D.S., and Zhang, L.M. 2013. Critical hydraulic gradients of internal erosion under complex stress states. Journal of Geotechnical and Geoenvironmental Engineering, 139(9), 1454-1467.

Chen, L., Zhao, J.C., Zhang, H.Y. and Lei, W. 2015. Experimental study on suffusion of gravelly soil. Soils Mechanics and Foundation Engineering, 52(3):135-143.

Chen, L., Lei, W., Zhang, H.Y., Zhao, J.C. and Li, J. 2013. Laboratory simulation and theoretical analysis of piping mechanism under unsteady flows. Chinese Journal of Geotechnical Engineering, 35(4):655-662.

Chen, L., Cai, G.D., Gu, J.H., Tan, Y.F., Chen, C. and Yin, Z.X. 2020. Effect of Clay on Internal Erosion of Clay-Sand-Gravel Mixture. Advance

in Civil Engineering,

https://doi.org/10.1155/2020/8869289

China (2015)http://www.chinanews.com/sh/2015/04-06/7186420.shtml

Fannin, R.J. and Moffat, R. 2006. Observations on internal stability of cohensionless soils. Geotechnique,56,497-500.

Foster, M., Fell, R. and Spannagle, M. 2000. The statistics of embankment dam failures and accidents. Canadian Geotechnical Journal, 37(5):1000–1024.

Hu, Z., Zhang, Y.D. and Yang, Z.X. 2020. Suffusion-Induced Evolution of Mechanical and Microstructural Properties of Gap-Graded Soils Using CFD-DEM. Journal of Geotechnical and Geoenvironmental Engineering, 146(5):04020024.

Huang, Z., Bai, Y.C., Xu, H.J., Cao, Y.F. and Hu, X. 2017. A Theoretical Model to Predict the Critical Hydraulic Gradient for Soil Particle Movement under Two-Dimensional Seepage Flow. Water, 9(11):828.

Ke, L. and Takahashi, A. 2012. Strength reduction of cohesionless soil due to internal erosion induced by one-dimensional upward seepage flow. Soils and Foundations, 52(4):698-711.

Kenney, T.C. and Lau, D. 1985. Internal stability of granular filters. Canadian Geotechnical Journal, 22(2):215-225.

Laos(2018)https://baijiahao.baidu.com/s?id=1606921771577827225&wfr=sp

ider&for=pc

Li, D., Zhou, N.Q., Wu, X.N. and Yin, J.C. 2020. Seepage–stress coupling response of cofferdam under storm surge attack in Yangtze estuary. Marine Georesources and Geotechnology, DOI: 10.1080/1064119X.2020.1712630

Liang, Y., Yeh, T-CJ., Zha, Y.Y., Wang, J.J., Liu, M.W. and Hao, Y.H. 2017. Onset of suffusion in gap-graded soils under upward seepage. Soils and Foundations, 57(5):849-860.

Liang, Y., Yeh, T-CJ., Zha, Y.Y., Wang, J.J., Liu, M.W. and Hao, Y.H. (2019) Onset of suffusion in upward seepage under isotropic and anisotropic stress conditions. European Journal of Environmental and Civil Engineering, 23(12):1520-1534.

Liang, X.Q. 1994. The situation and value of flood control of Beijiang dike in 1994. Guangdong Water Resources and Hydropower, 4: 31-34.

Lu, T.H. 2005. Soils Mechanics[M]. (second edition) hohai university press, 102-103.

Luo, Y.L., Wu, Q., Zhan, M.L., Sheng, J.C. 2013. Development of seepage-erosion-stress coupling piping test apparatus and its primary application. Chinese Journal of Rock Mechanics and Engineering, 32(10):2108–2114.

Mao, C.X., Duan, X.B., and Wu, L.J. 2009. Study of critical gradient

of piping for various grain sizes in sandy gravels. Rock and Soil Mechanics, 30(12): 3705-3709.

Mao, C.X., Duan, X.B. and Cai, J.B. 2005. Piping experimental study and theoretical analysis of unsteady seepage flow during flood peak. Journal of Hydraulic Engineering, 36(9): 1105 - 1120.

Mao, C.X., Duan, X.B. and Cai, J.B. 2005. Experimental study and analysis on piping of levee in Beijiang River. Journal of Hydraulic Engineering, 36(7):818-824.

Mao, C.X., Duan, X.B. and Cai, J.B. 2004. Experimental study on harmless seepage piping in levee foundation. Journal of Hydraulic Engineering, 36(7):46-53.

Mao, C.X. 2013. Dam Engineering Hydraulics and Design Management [M]. Water Resources and Electric Power Press.

McDougall, J-Kelly-D. and Barreto, D. 2013. Particle loss and volume change on dissolution: Experimental results and analysis of particle size and amount effects. Acta Geotechnica, 8, 619–627. doi:10.1007/s11440-013-0212-0.

Razavi, S.K., Bonab, M.H. and Dabaghian, A. 2020. Investigation into the Internal Erosion and Local Settlement of Esfarayen Earth-Fill Dam. Journal of Geotechnical and Geoenvironmental Engineering, 146(4): 04020006.

Richards, K.S. and Reddy, K.R. 2007. Critical appraisal of piping phenomena in earth dams. Bulletin of Engineering Geology and the Environment, 66(4):381–402.

Schuler, U. 1995. How to deal with the problem of suffusion[C]//Research and Development in the Field of Dams. Switzerland: [s. n.]:145-159.

Skempton, A. W. and Brogan, J. M. 1994. Experiments on piping in sandy gravels. Geotechnique, 44, 449–460.

Uzbekistan (2020) https://mini.eastday.com/a/200512130123540.html

Vandenboer, K., Celette, F. and Bezuijen, A. 2019. The effect of sudden critical and supercritical hydraulic loads on backward erosion piping: small-scale experiments. Acta Geotechnica, 14:783–794.

Wan, C.F. and Fell, R. 2008. Assessing the potential of internal instability and suffusion in embankment dams and their foundations. Journal of Geotechnical and Geoenvironmental Engineering, 134(3):401-407.

Wang T, Chen J, Wang T, Wang S. 2015. Entropy weight-set pair analysis based on tracer techniques for dam leakage investigation. Natural Hazards, 76(2): 747–767.

Xie, Q.Y., Liu, J., Han, B., Li, H.T., Li, Y.Y. and Li, X.Z. 2018. Critical Hydraulic Gradient of Internal Erosion at the Soil–Structure

Interface. Processes, 6(7), 92; doi:10.3390/pr6070092

Yang, K.H. and Wang, J.Y. 2017. Experiment and statistical assessment on piping failures in soils with different gradations. Marine Georesources and Geotechnology, 35(4):512-527.

Zeng, C. 2016. Experimental study on piping erosion mechanism of cohesionless soil. Master thesis, Chong-qing Jiaotong University

Zhang, D.M., Du, W.W., Peng, M.Z., Feng, S.J. and Li, Z.L. 2020. Experimental and numerical study of internal erosion around submerged defective pipe. Tunnelling and Underground Space Technology, 97:103256.

Zhang, W.J. 2013. Fluid Mechanics[M]. China Architecture & Building Press, 2013.

Zou, Y.H., Chen, C. and Zhang, L.M. 2020. Simulating Progression of Internal Erosion in Gap-Graded Sandy Gravels Using Coupled CFD-DEM. International Journal of Geomechanics, 20(1): 04019135.

Fig. 1. Size distribution of the samples

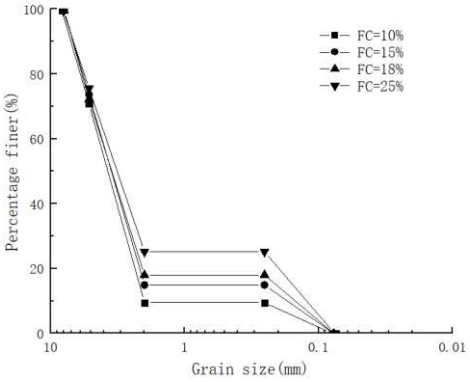

Fig. 2. Schematic diagram of the piping device: (a) Apparatus of the model tests and (b) Data acquisition system.

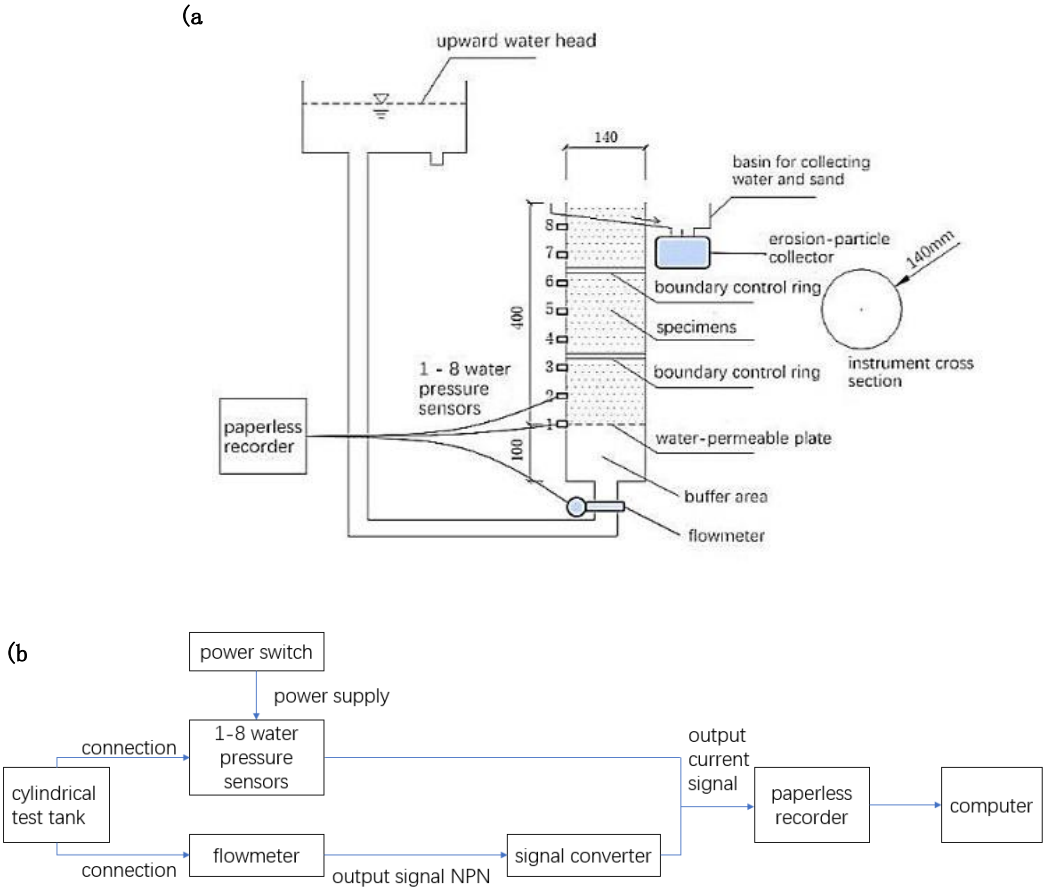

Fig. 3. Dr0.6 saturation sample: (a) Top surface of the sample and (b) Side of the sample.

(a  (b 

Fig. 4. Dr0.6 upstream water head lifting stage: (a) Changes in the seepage quantity and pore pressure; (b) Point A (26 min); (c) Point B (32 min); (d) Point C (47 min); (e) Point D (57 min).

(a

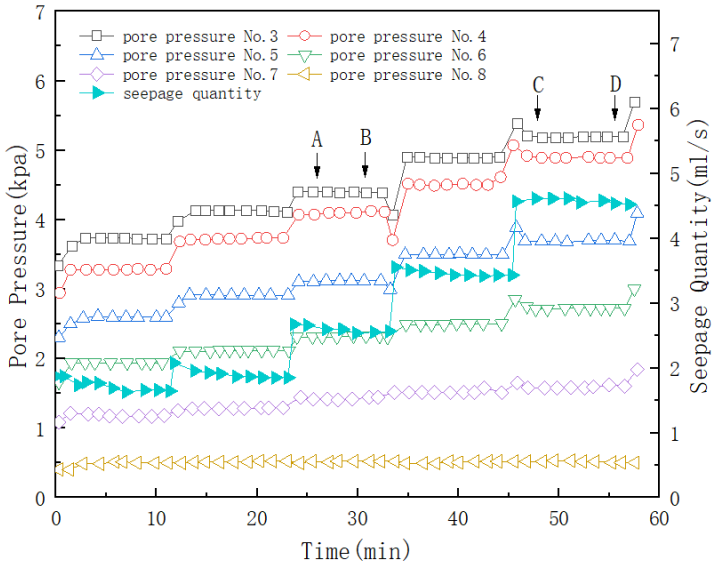

(b  (c 

(d

(e

Fig. 5. Process of Dr0.6 piping failure: (a) Changes in the seepage quantity and pore pressure; (b) Point E (193 min); (c) Point F (268 min); (d) Point G (575 min); (e) Point H (695 min); (f) Side of the sample (695 min).

(a

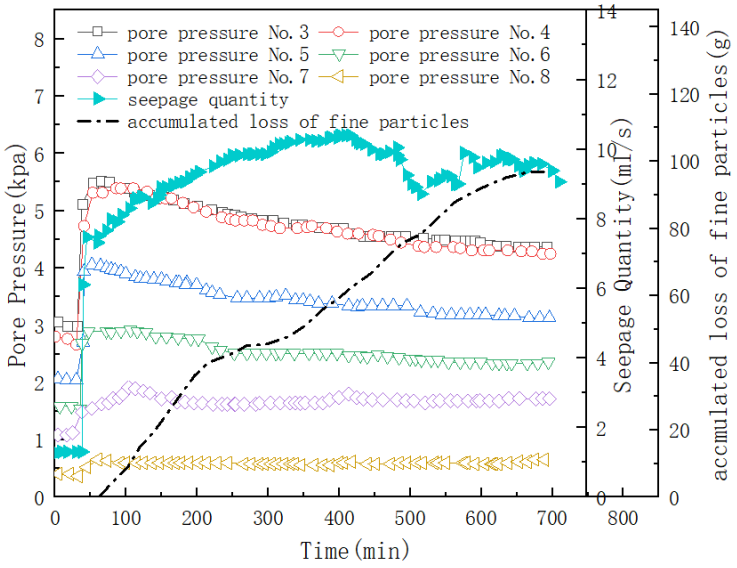

(b

(c

(d

(e

(f

Fig. 6. Variation in the velocity with time: (a) Dr group and (b) FC group.

(a

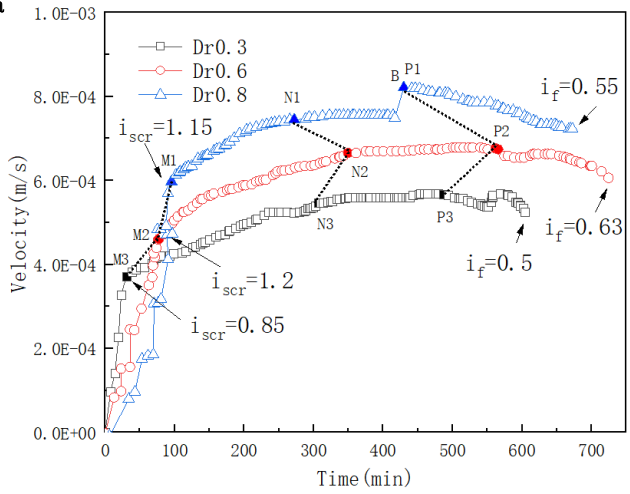

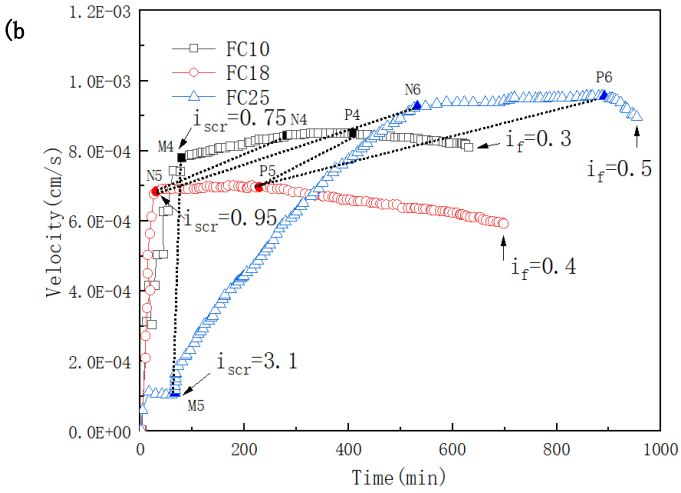

Fig. 7. Dr0.6 variation in the velocity with time

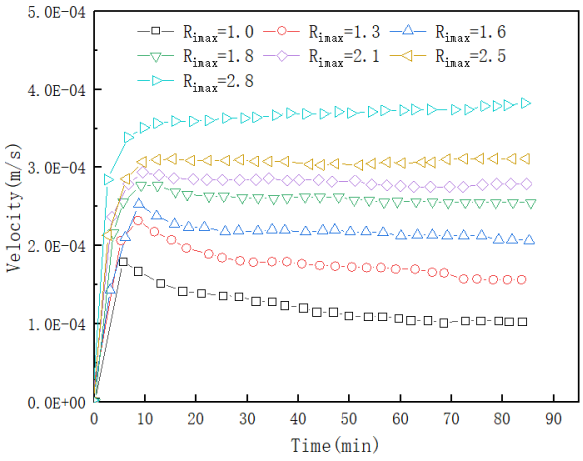

Fig. 8. Distribution of the flow velocity state with the change in various SCHGs: (a) Dr group and (b) FC group.

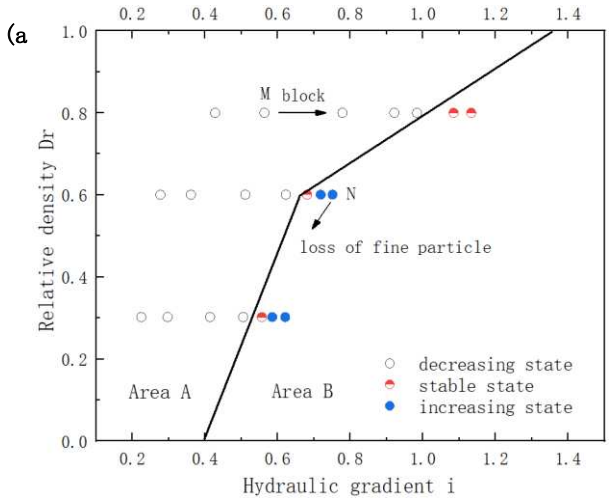

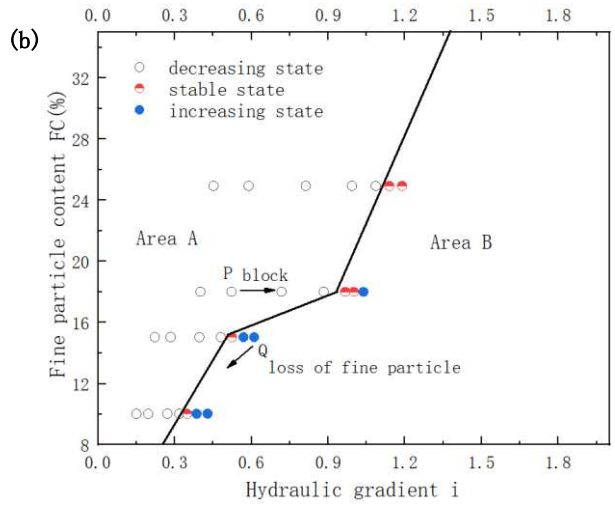

Fig. 9. Distribution of the flow velocity state with the change in R_i: (a) Dr group and (b) FC group.

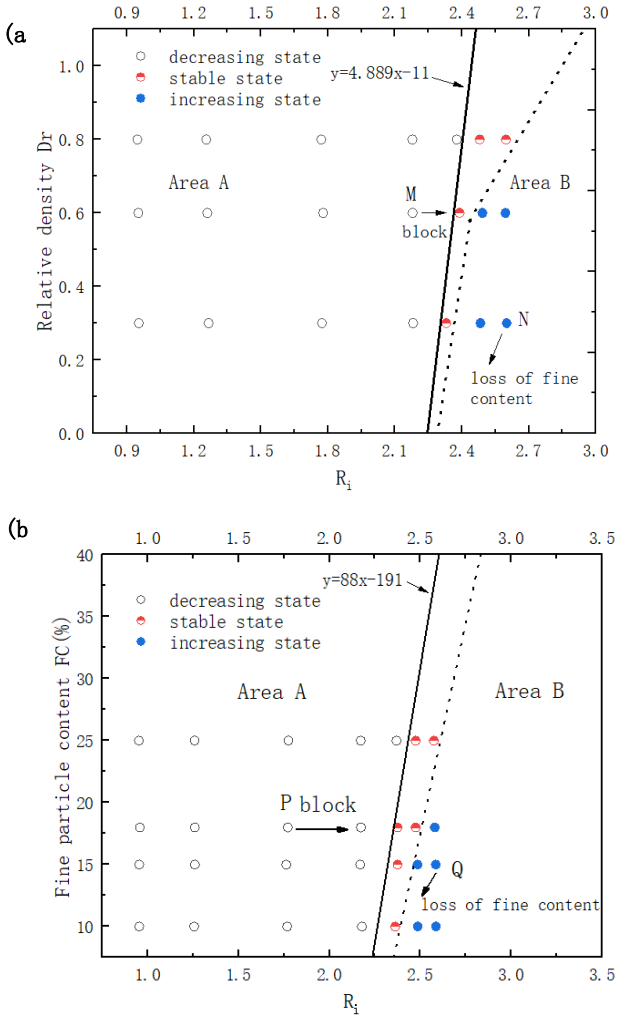

Fig. 10. Change path of the flow velocity state during the whole process of piping erosion: (a) Dr group and (b) FC group.

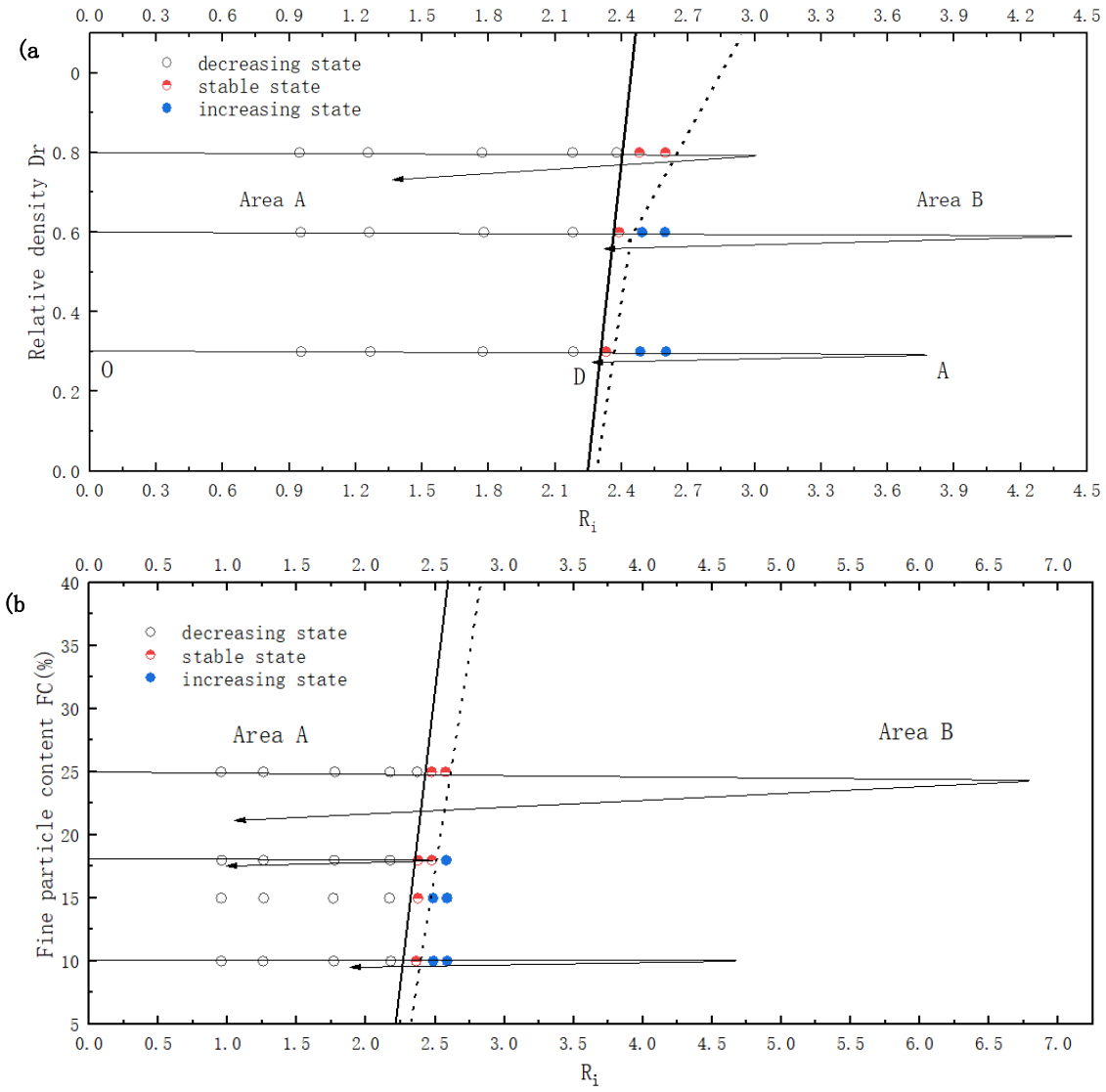

Fig. 11. Variation in the velocity with R_i: (a) Dr group and (b) FC group.

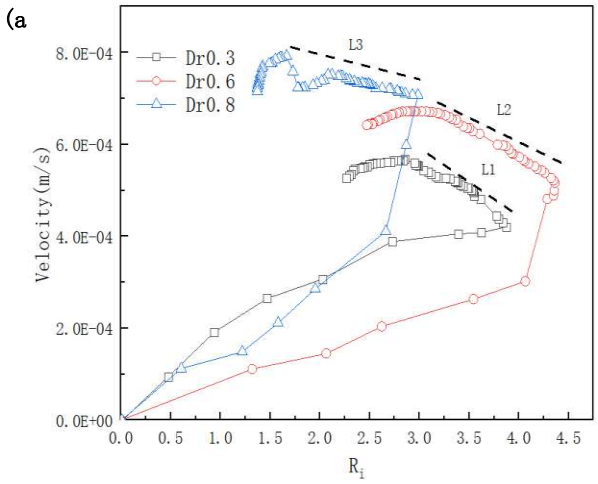

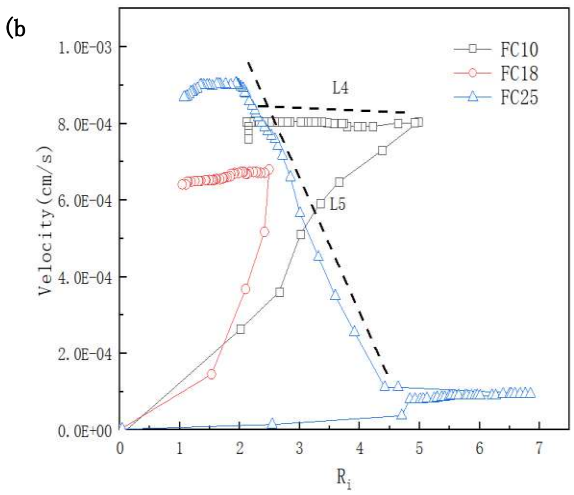

Fig. 12. Variation in the hydraulic conductivity with time: (a) Dr group and (b) FC group.

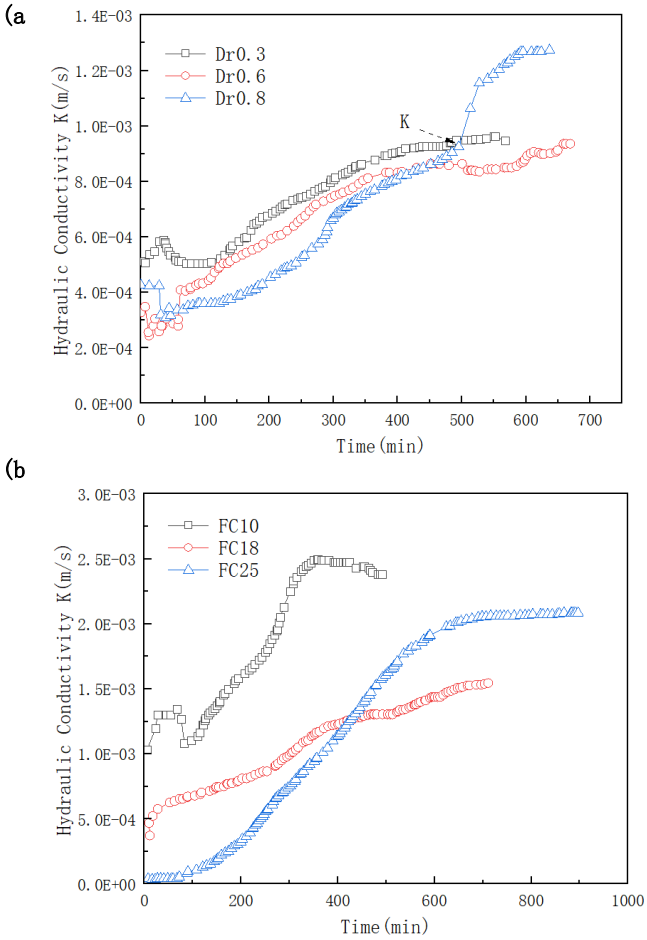

Fig. 13. Variation in the hydraulic conductivity with R_i: (a) Dr group and (b) FC group.

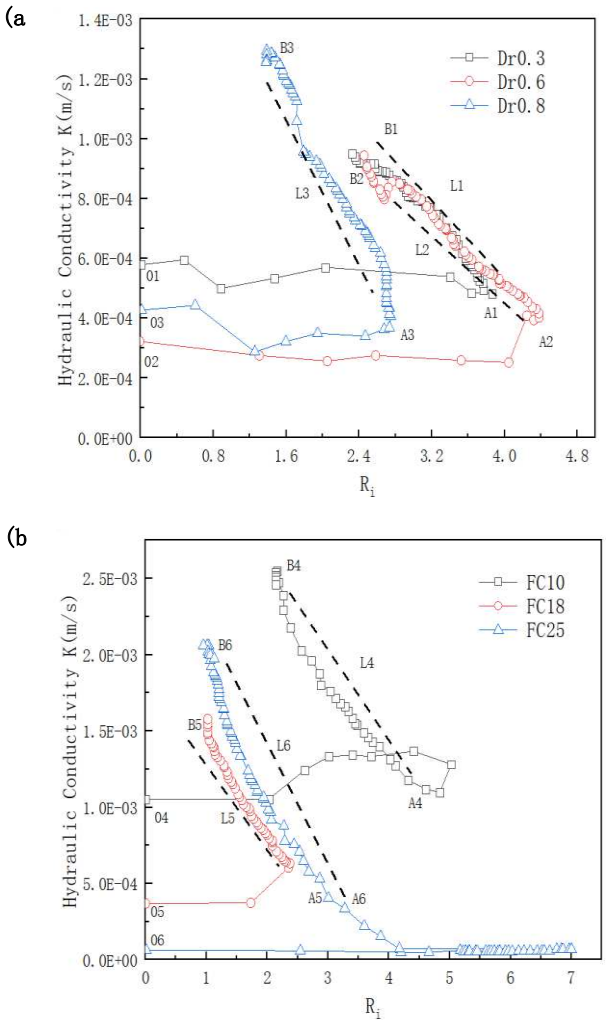

Fig. 14. Loss of fine particles in different stages of piping erosion

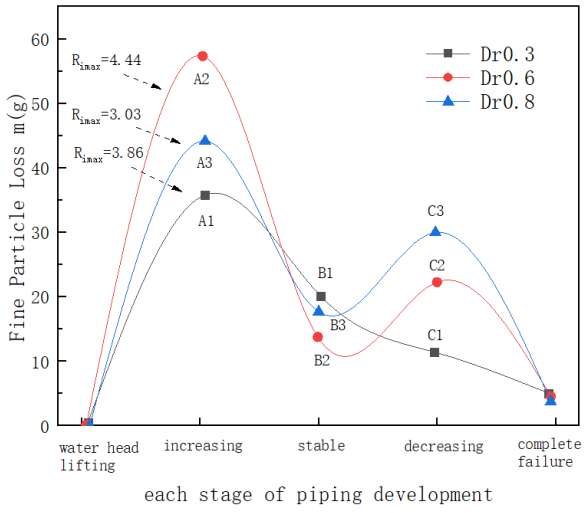

Fig. 15. Flood peak process line: (a)Real flood peak process line and (b) Simplified flood peak process line.

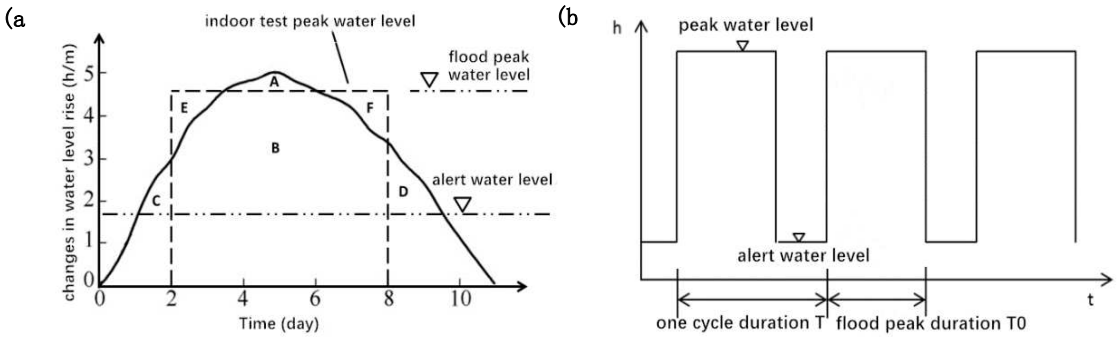

Fig. 16 Variation in the flow velocity with time: (a) FC10 group; (b) FC18 group; (c) FC25 group; (d) Dr0.3; (e) Dr0.6; (f) Dr0.8.

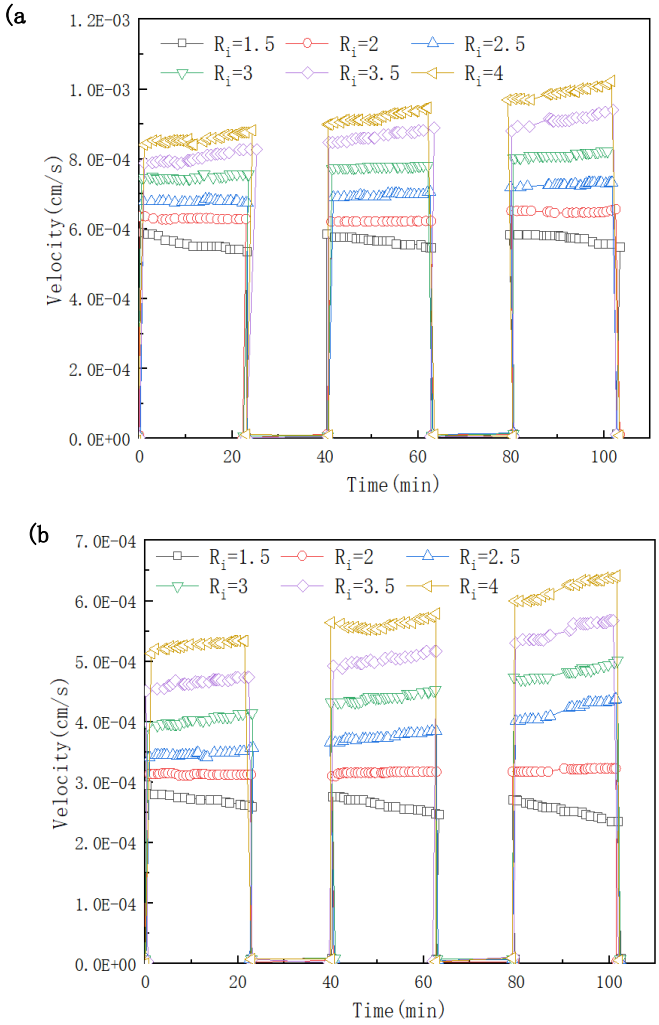

(c

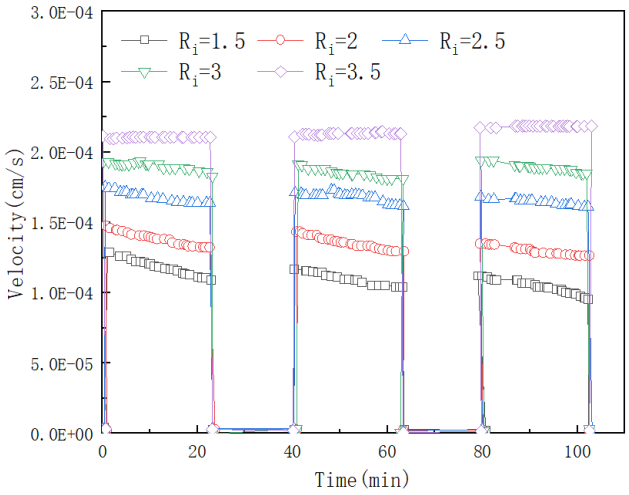
3.0E-04
2.5E-04
2.0E-04
1.5E-04
1.0E-04
5.0E-05
0.0E+00
Velocity(cm/s)
0
20
40
60
80
100
Time(min)
Ri=1.5
Ri=2
Ri=2.5
Ri=3
Ri=3.5

(d

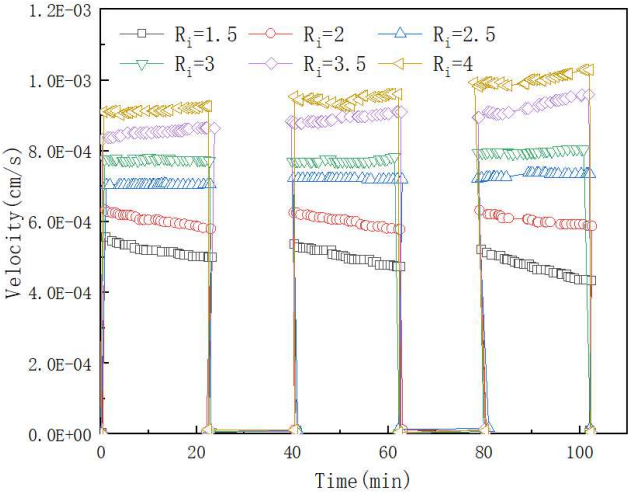
1.2E-03
1.0E-03
8.0E-04
6.0E-04
4.0E-04
2.0E-04
0.0E+00
Velocity(cm/s)
0
20
40
60
80
100
Time(min)
Ri=1.5
Ri=2
Ri=2.5
Ri=3
Ri=3.5
Ri=4

(e

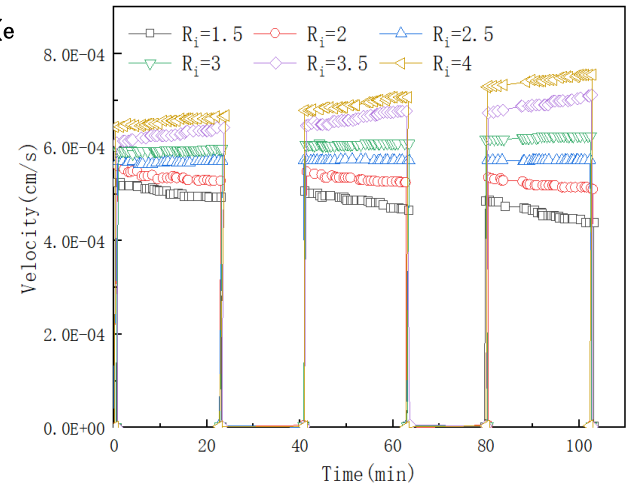
8.0E-04
6.0E-04
4.0E-04
2.0E-04
0.0E+00
Velocity(cm/s)
0
20
40
60
80
100
Time(min)
Ri=1.5
Ri=2
Ri=2.5
Ri=3
Ri=3.5
Ri=4

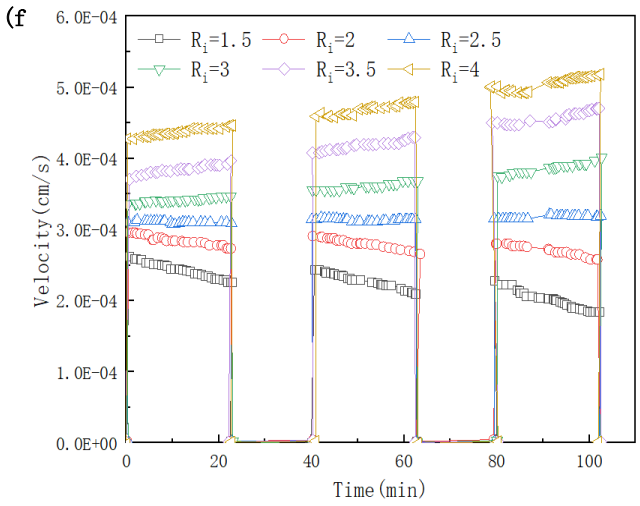

Fig. 17 Variation in the velocity with R_i: (a) FC group and (b) Dr group.

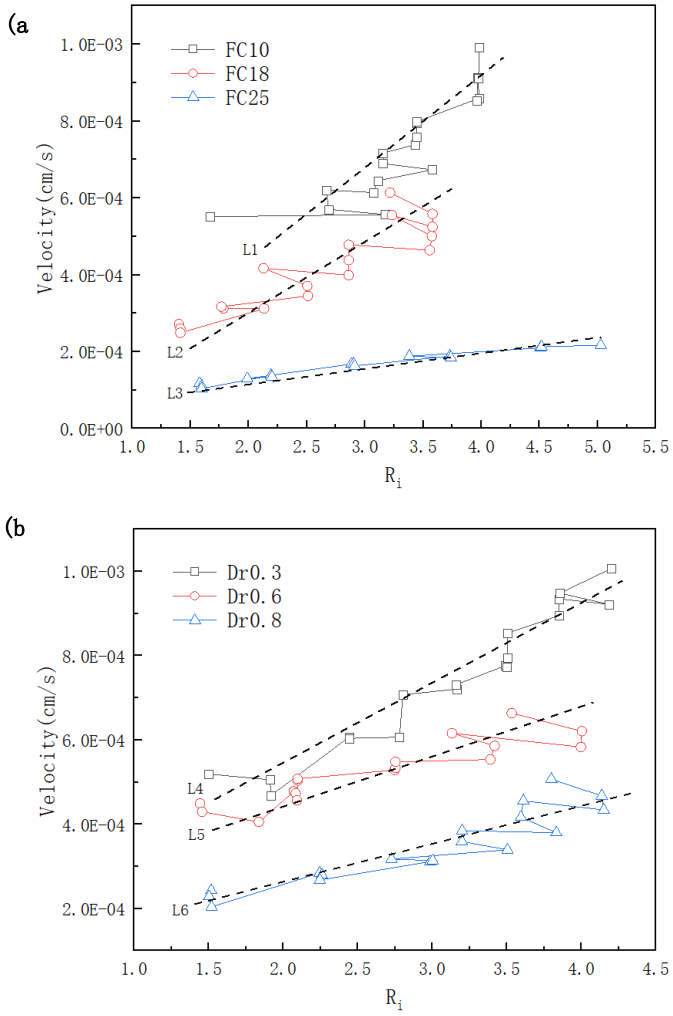

Fig. 18 Comparison of the variation in the flow velocity with R_i: (a) FC10 group; (b) FC18 group; (c) FC25 group; (d) Dr0.3 group; (e) Dr0.6 group; (f) Dr0.8 group.

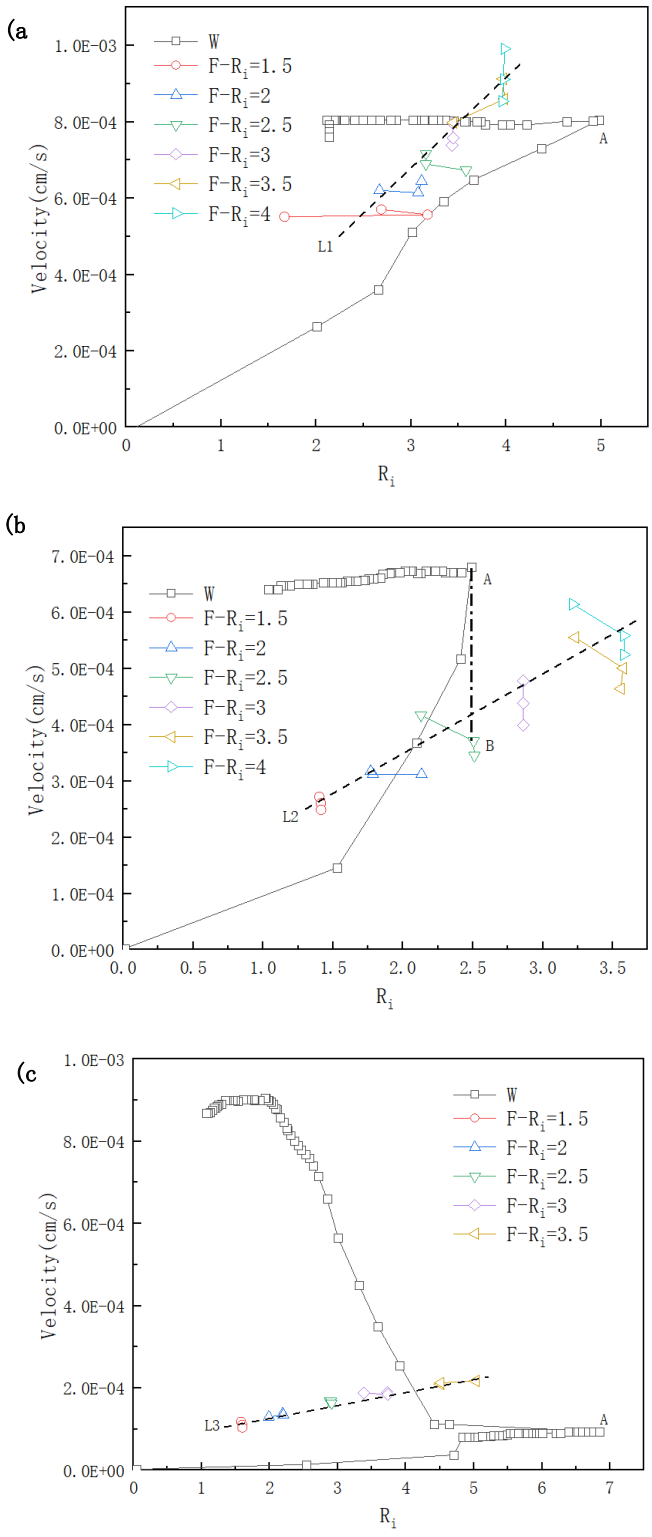

(d

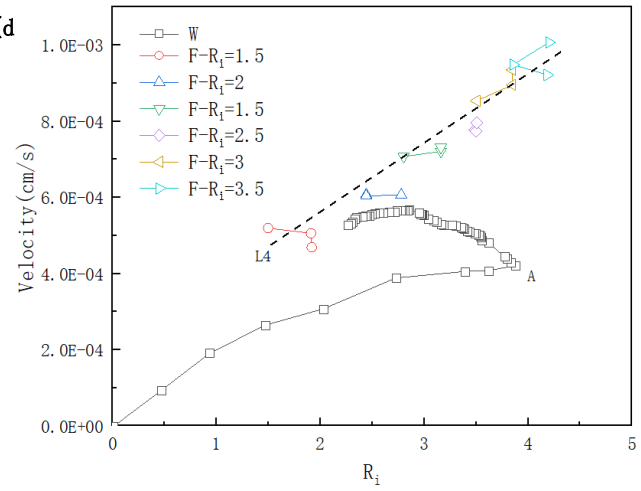
W
F-R$_i$=1.5
F-R$_i$=2
F-R$_i$=1.5
F-R$_i$=2.5
F-R$_i$=3
F-R$_i$=3.5
L4
A
Velocity(cm/s)
R$_i$

(e

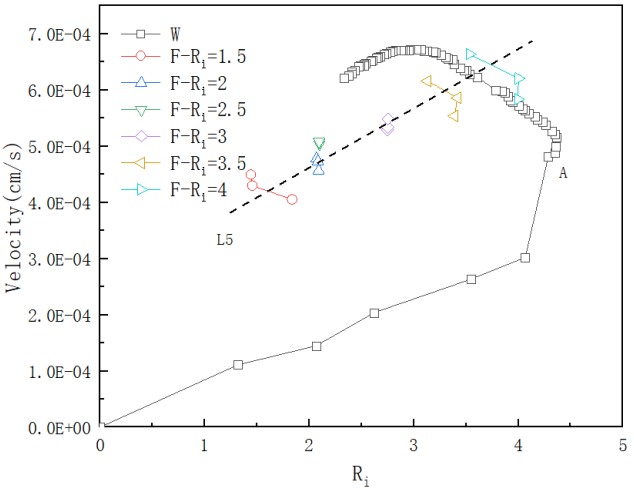
W
F-R$_i$=1.5
F-R$_i$=2
F-R$_i$=2.5
F-R$_i$=3
F-R$_i$=3.5
F-R$_i$=4
L5
A
Velocity(cm/s)
R$_i$

(f

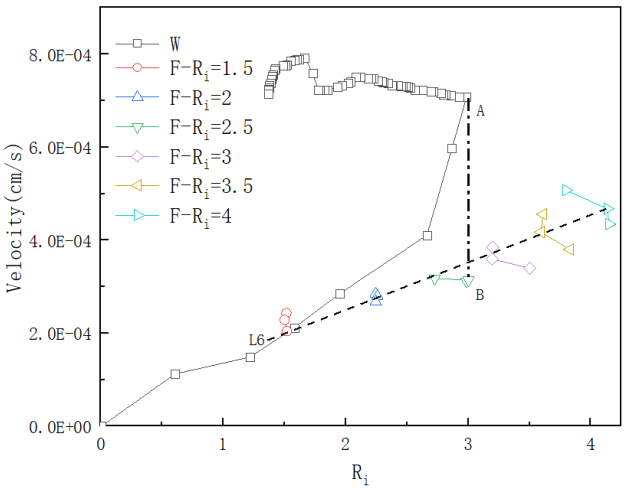
W
F-R$_i$=1.5
F-R$_i$=2
F-R$_i$=2.5
F-R$_i$=3
F-R$_i$=3.5
F-R$_i$=4
A
B
L6
Velocity(cm/s)
R$_i$

Table 1 Test scheme and materials physical properties

Sample	Number	Initial fines content FC (%)	Maximum void ratio e_{max}	Minimum void ratio e_{min}	Initial relative density Dr	Length L (cm)	Specific gravity Gs
FC	FC10	10%	0.59	0.39	0.3	25	2.70
	FC18	18%	0.54	0.28	0.3	25	2.70
	FC25	25%	0.50	0.26	0.3	25	2.70
Dr	Dr0.3	15%	0.56	0.29	0.3	25	2.70
	Dr0.6	15%	0.56	0.29	0.6	25	2.70
	Dr0.8	15%	0.56	0.29	0.8	25	2.70

Table 2 Fixed SCHG i_{scr}, failure hydraulic gradient i_f and CHG of the sample

Sample	i_{scr}	i_f	i_{cr}	$R_{imax}=i_{scr}/i_{cr}$
Dr0.3	0.85	0.5	0.22	3.86
Dr0.6	1.2	0.63	0.35	4.44
Dr0.8	1.15	0.55	0.4	3.03
FC10	0.75	0.3	0.16	4.69
FC18	0.95	0.4	0.4	2.38
FC25	3.1	0.5	0.45	6.89

Table 3 The circulating water head duration of the model

Seepage length Lm (mm)	Time scale λ_t	Flood peak water level duration Tm0 (min)	Alerted water level duration Tm1 (min)	Entire cycle duration Tm (min)
250	400	22	18	40

Figures

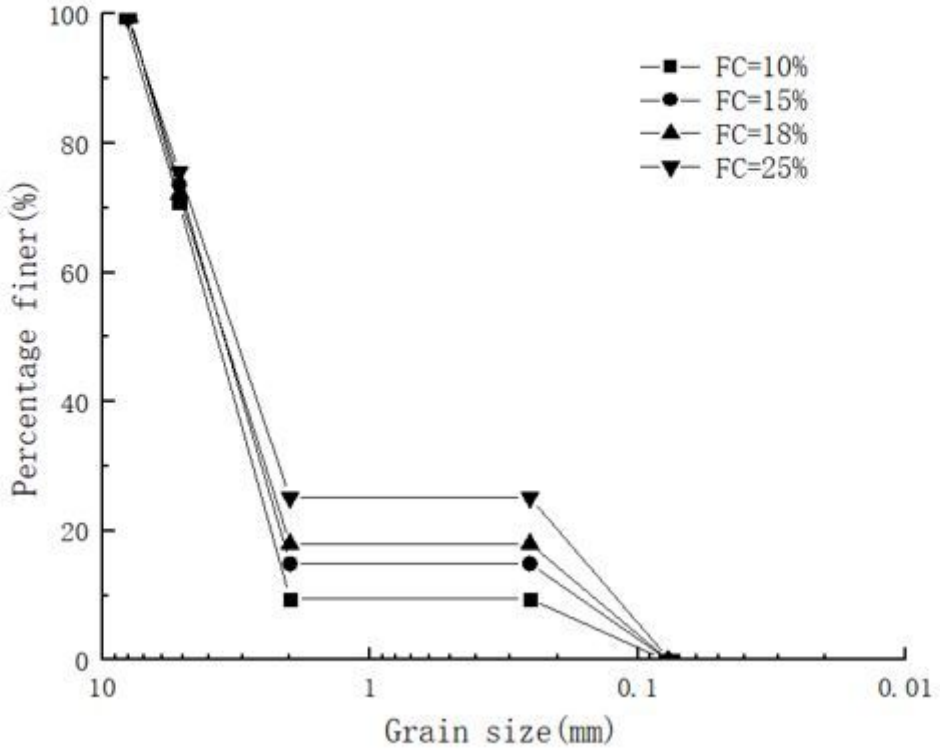

Figure 1

Size distribution of the samples

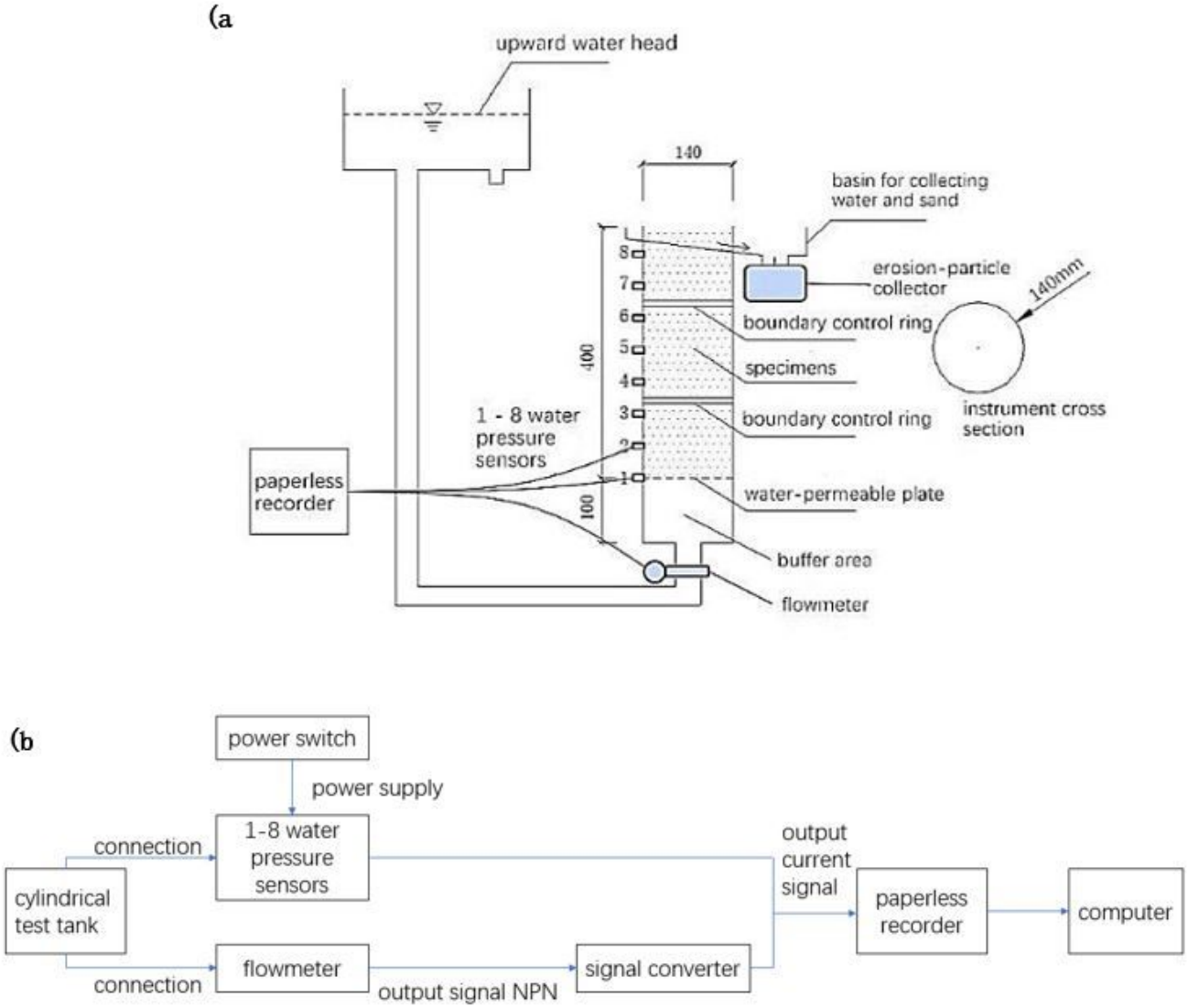

Figure 2

Schematic diagram of the piping device (a) Apparatus of the model tests and (b) Data acquisition system.

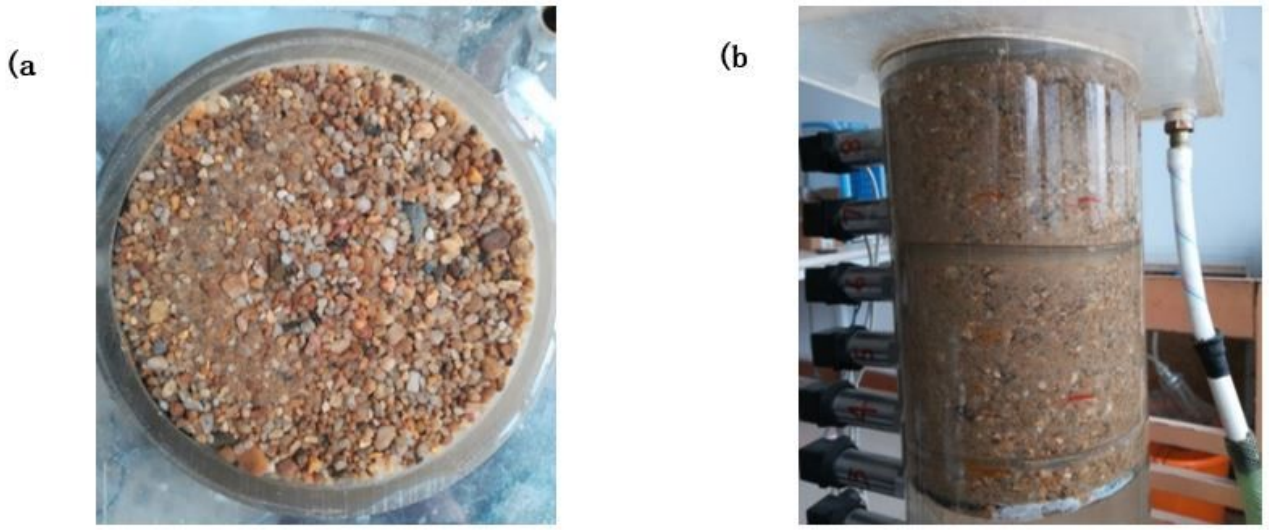

Figure 3

Dr0.6 saturation sample: (a) Top surface of the sample and (b) Side of the sample.

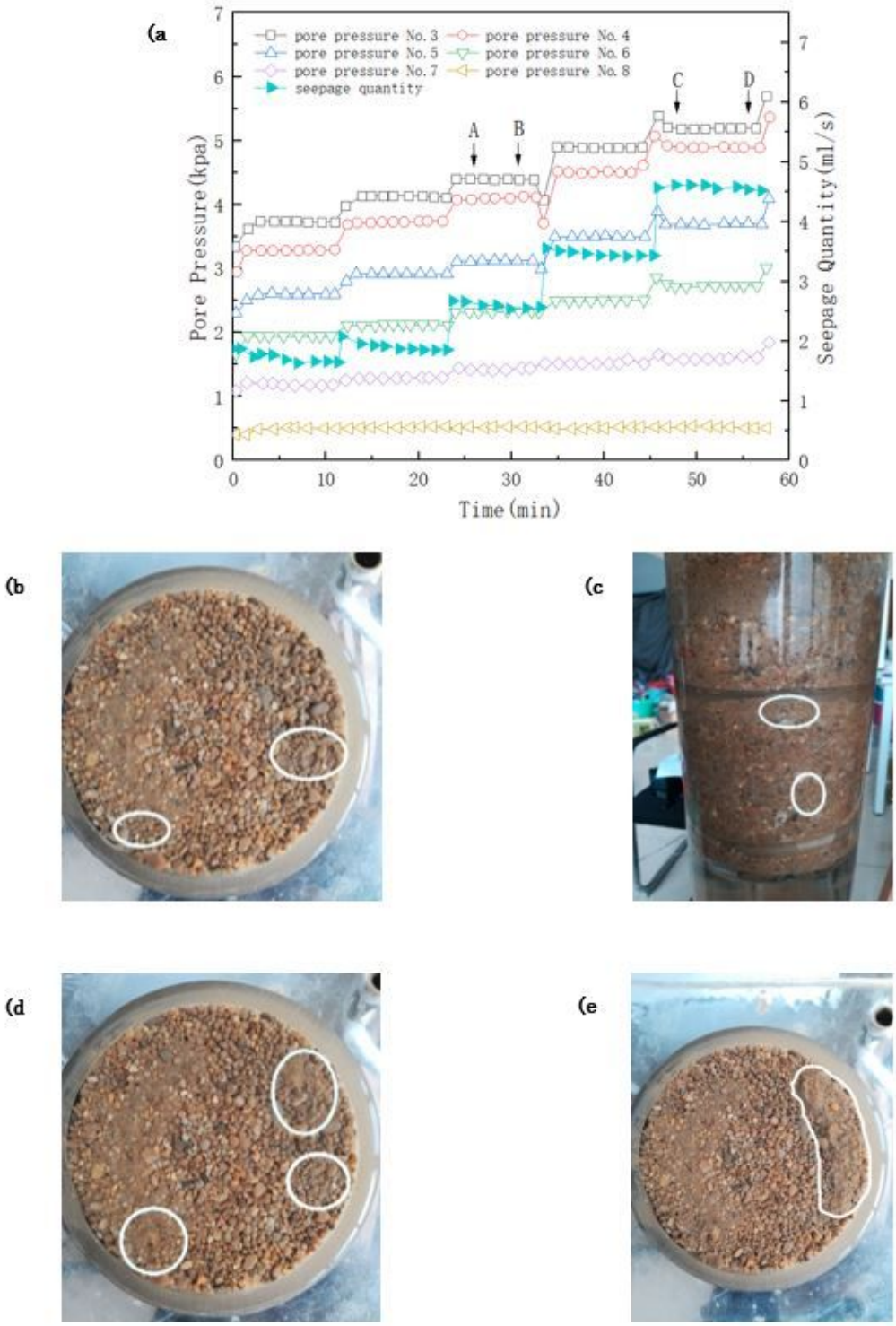

Figure 4

Dr0.6 upstream water head lifting stage: (a) Changes in the seepage quantity and pore pressure; (b) Point A (26 min); (c) Point B (32 min); (d) Point C (47 min); (e) Point D (57 min).

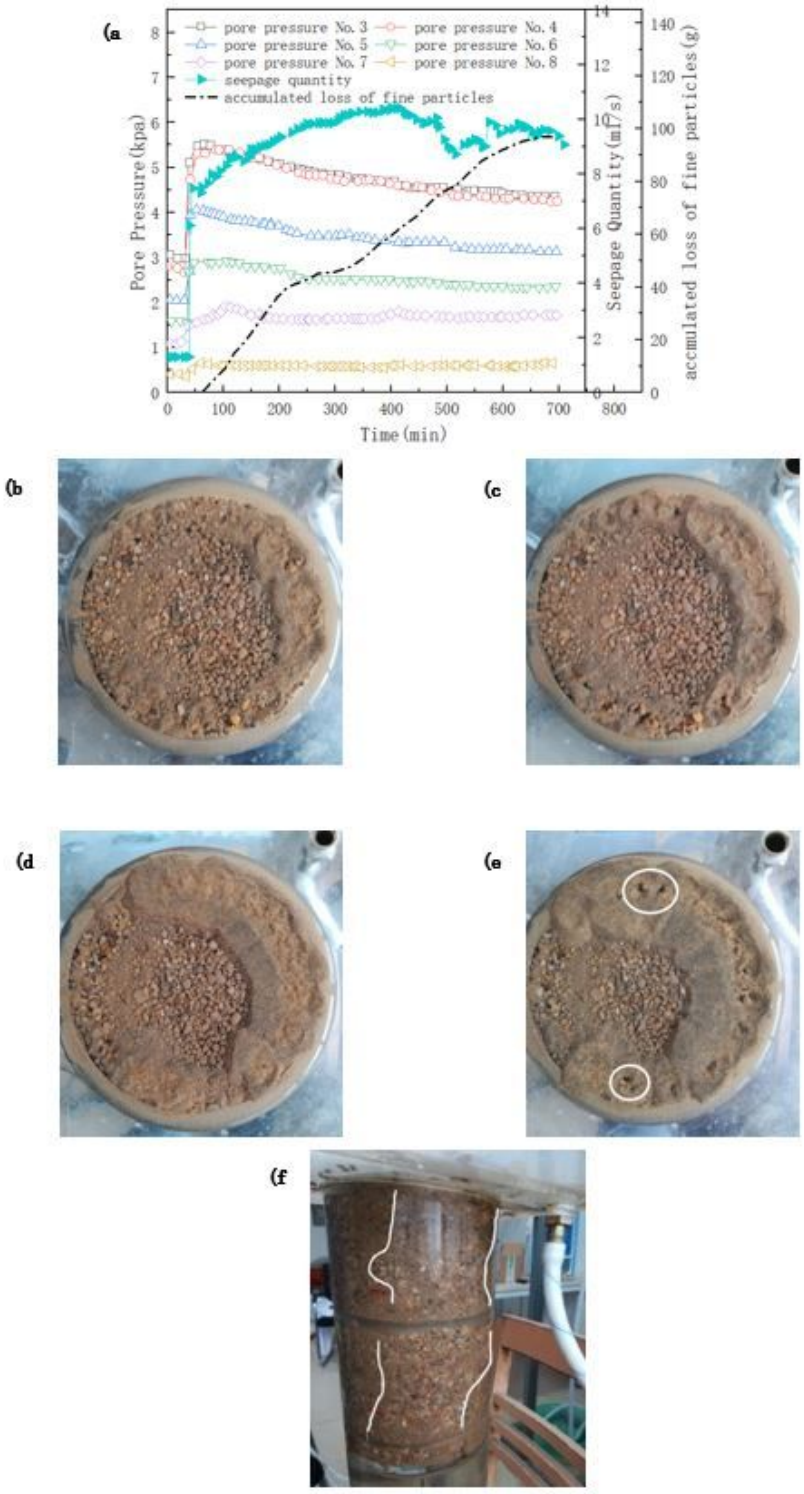

Figure 5

Process of Dr0.6 piping failure: (a) Changes in the seepage quantity and pore pressure; (b) Point E (193 min); (c) Point F (268 min); (d) Point G (575 min); (e) Point H (695 min); (f) Side of the sample (695 min).

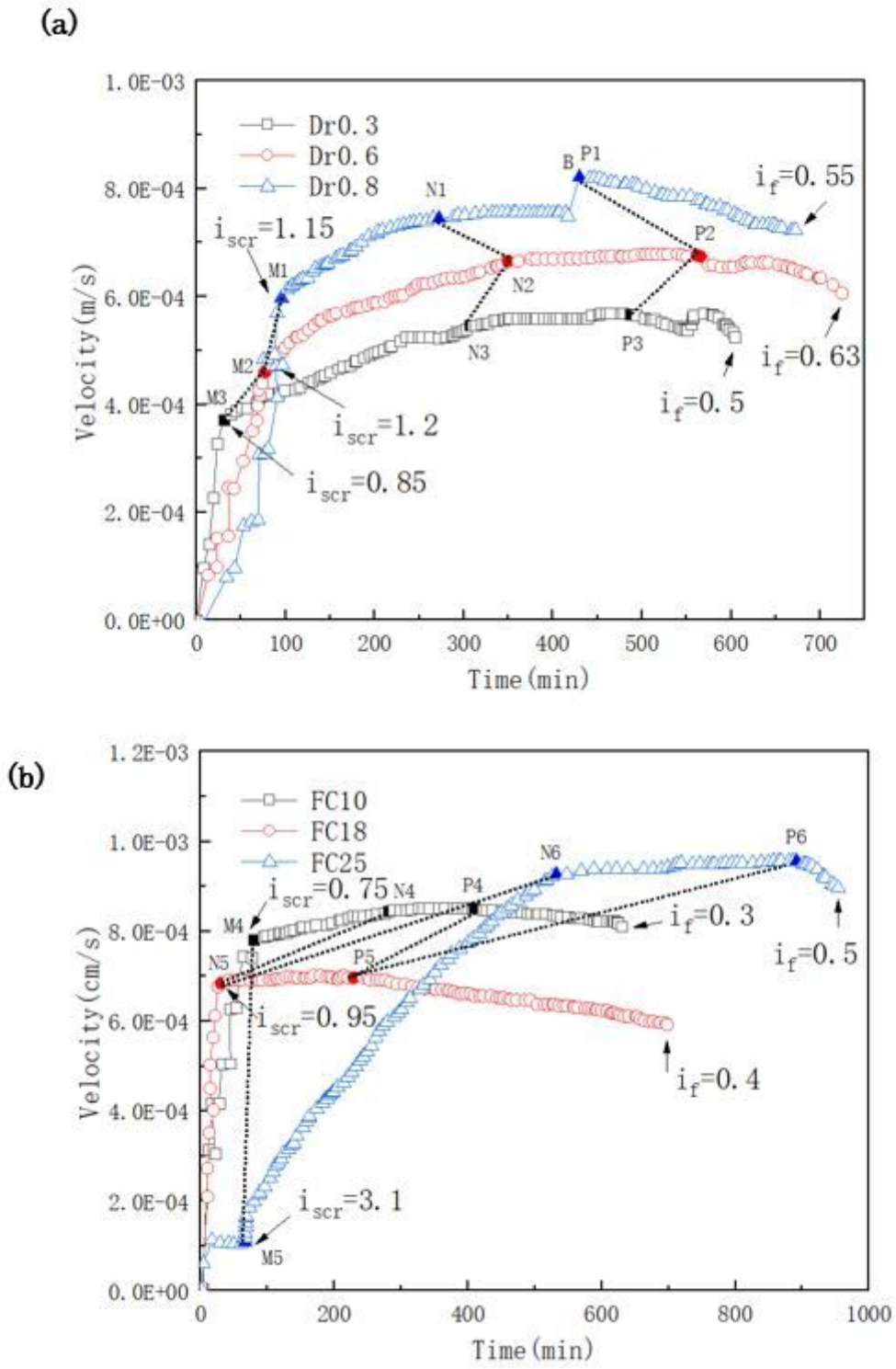

Figure 6

Variation in the velocity with time: (a) Dr group and (b) FC group.

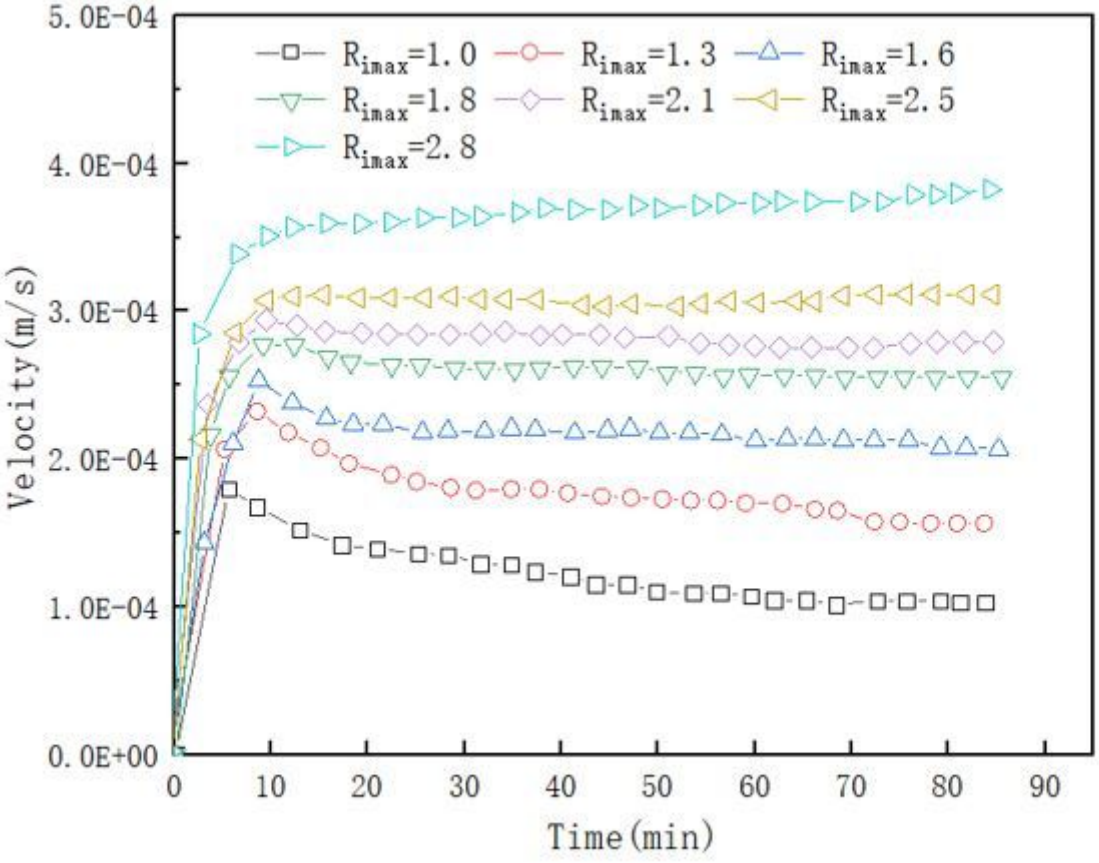

Figure 7

Dr0.6 variation in the velocity with time

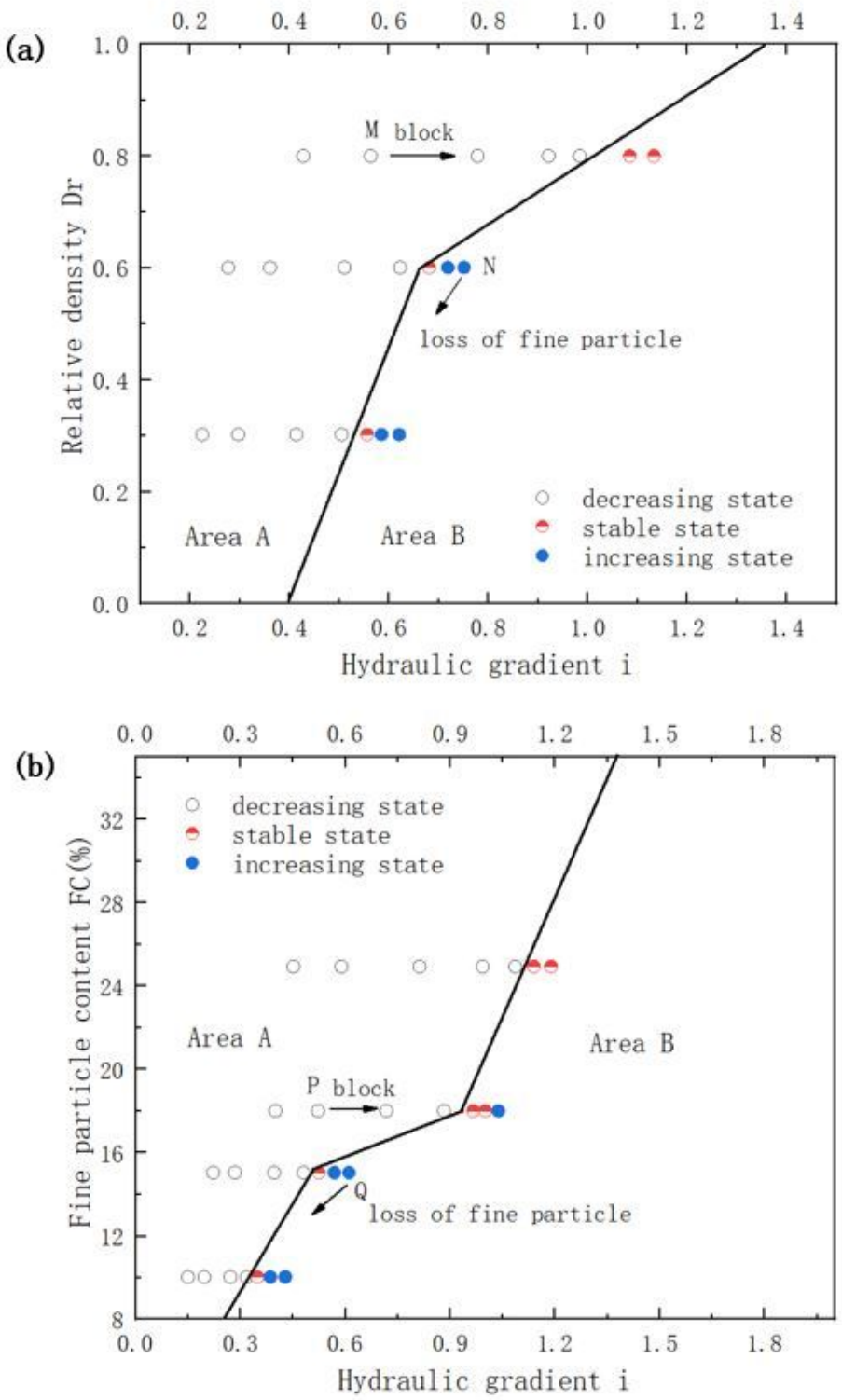

Figure 8

Distribution of the flow velocity state with the change in various SCHGs: (a) Dr group and (b) FC group.

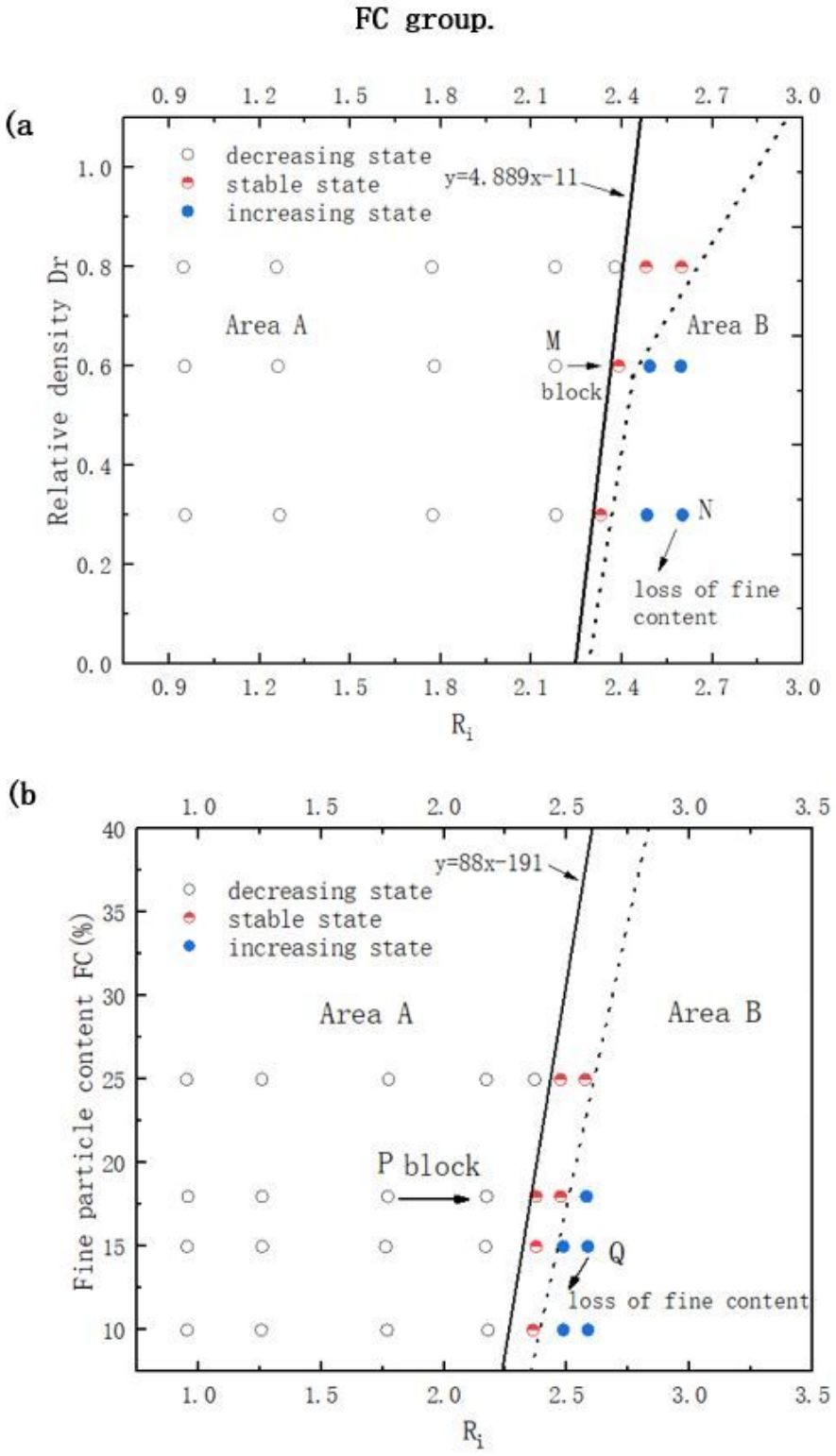

Figure 9

Distribution of the flow velocity state with the change in Ri: (a) Dr group and (b) FC group.

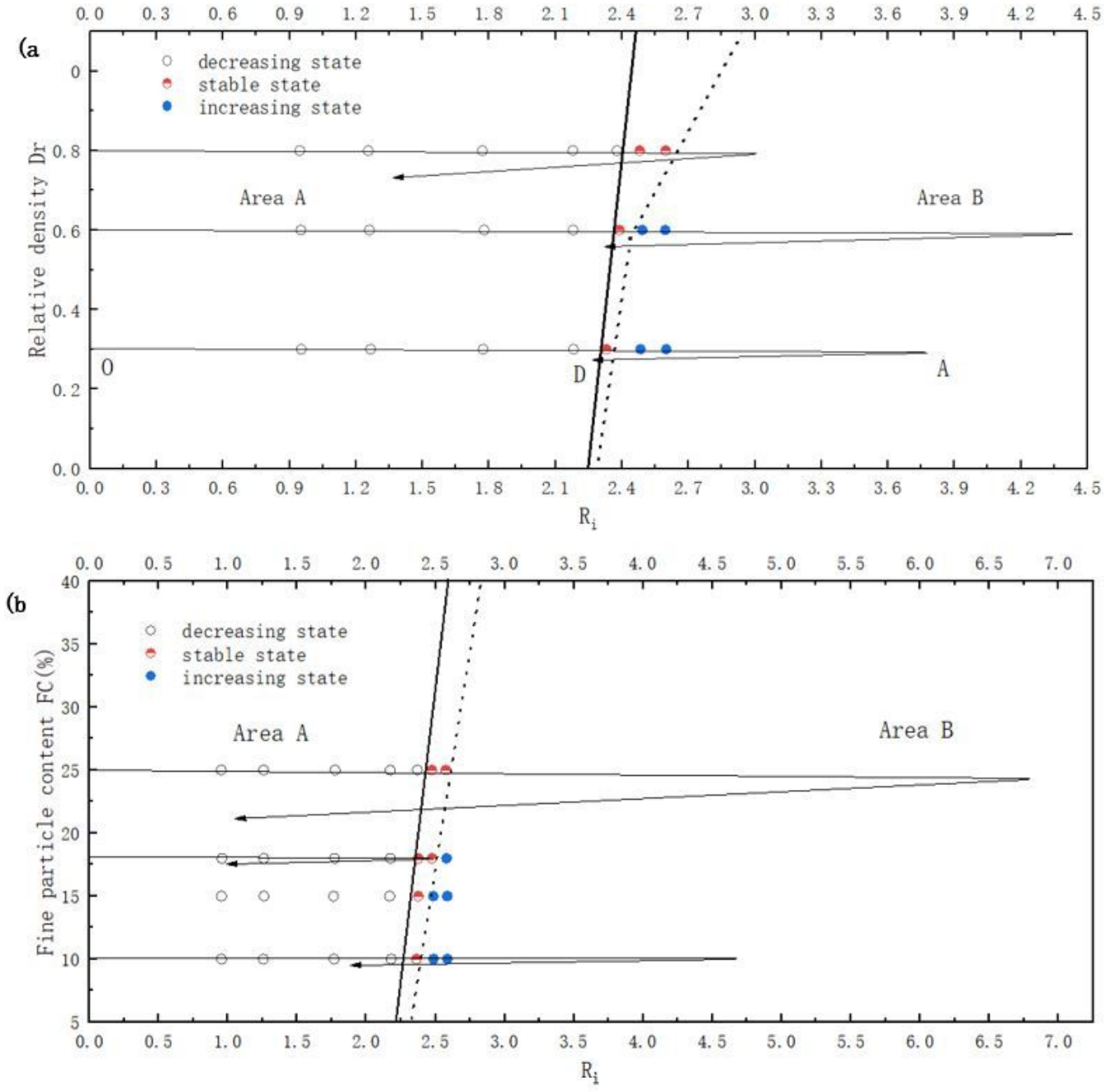

Figure 10

Change path of the flow velocity state during the whole process of piping erosion: (a) Dr group and (b) FC group.

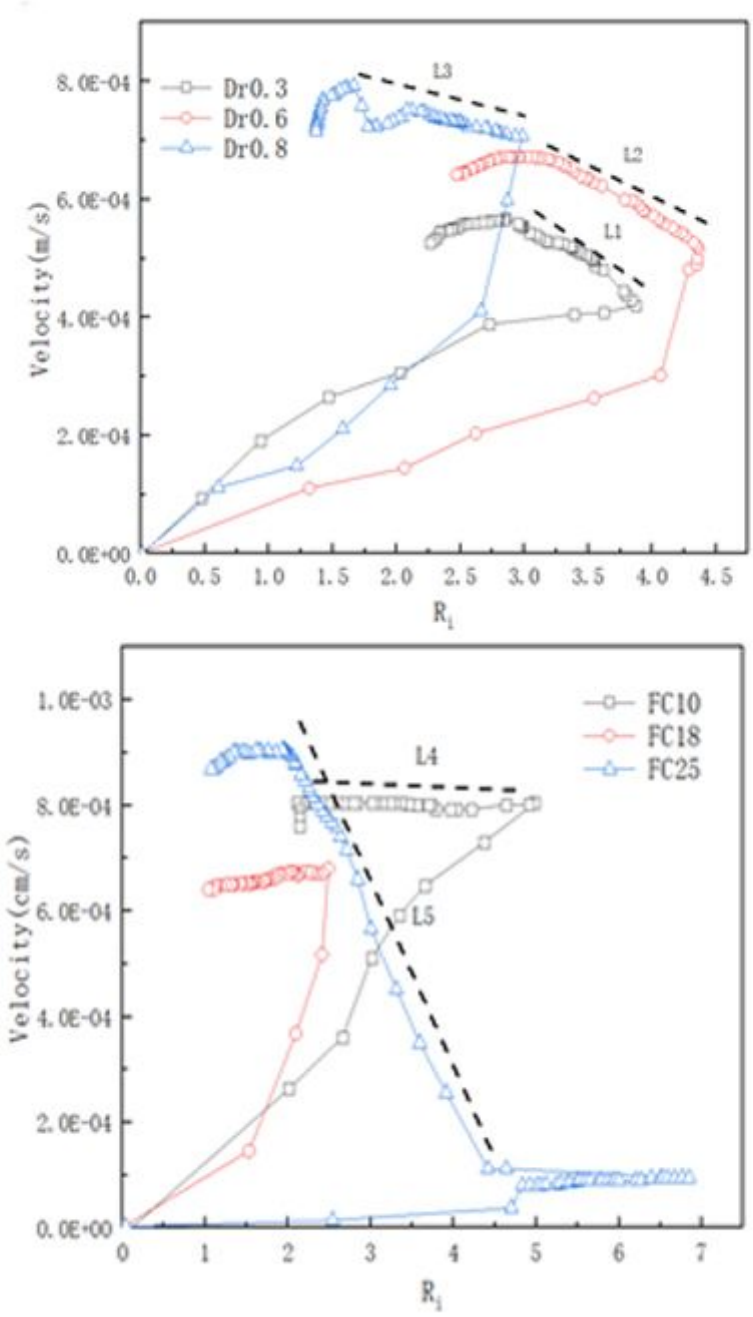

Figure 11

Variation in the velocity with Ri: (a) Dr group and (b) FC group.

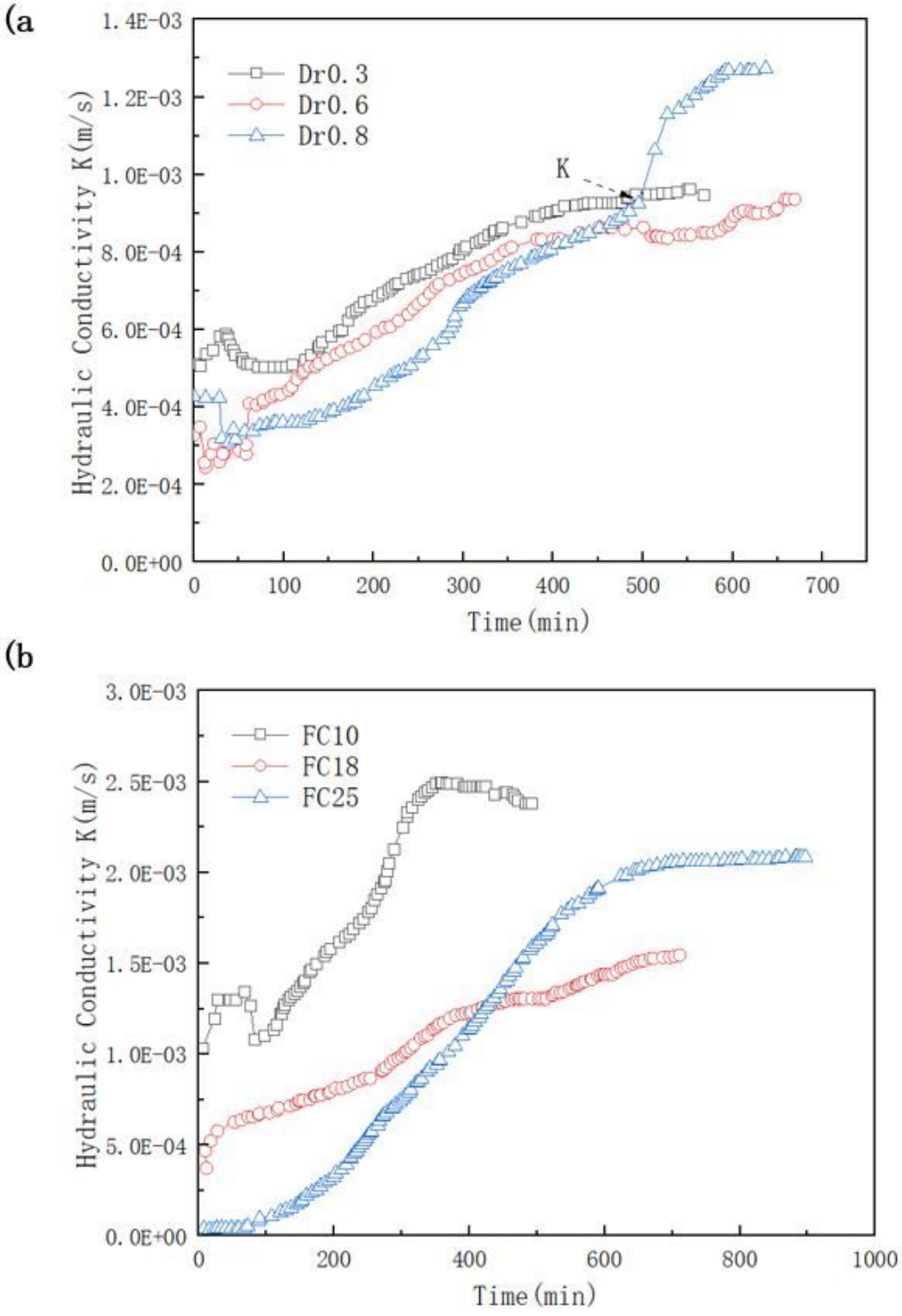

Figure 12

Variation in the hydraulic conductivity with time: (a) Dr group and (b) FC group.

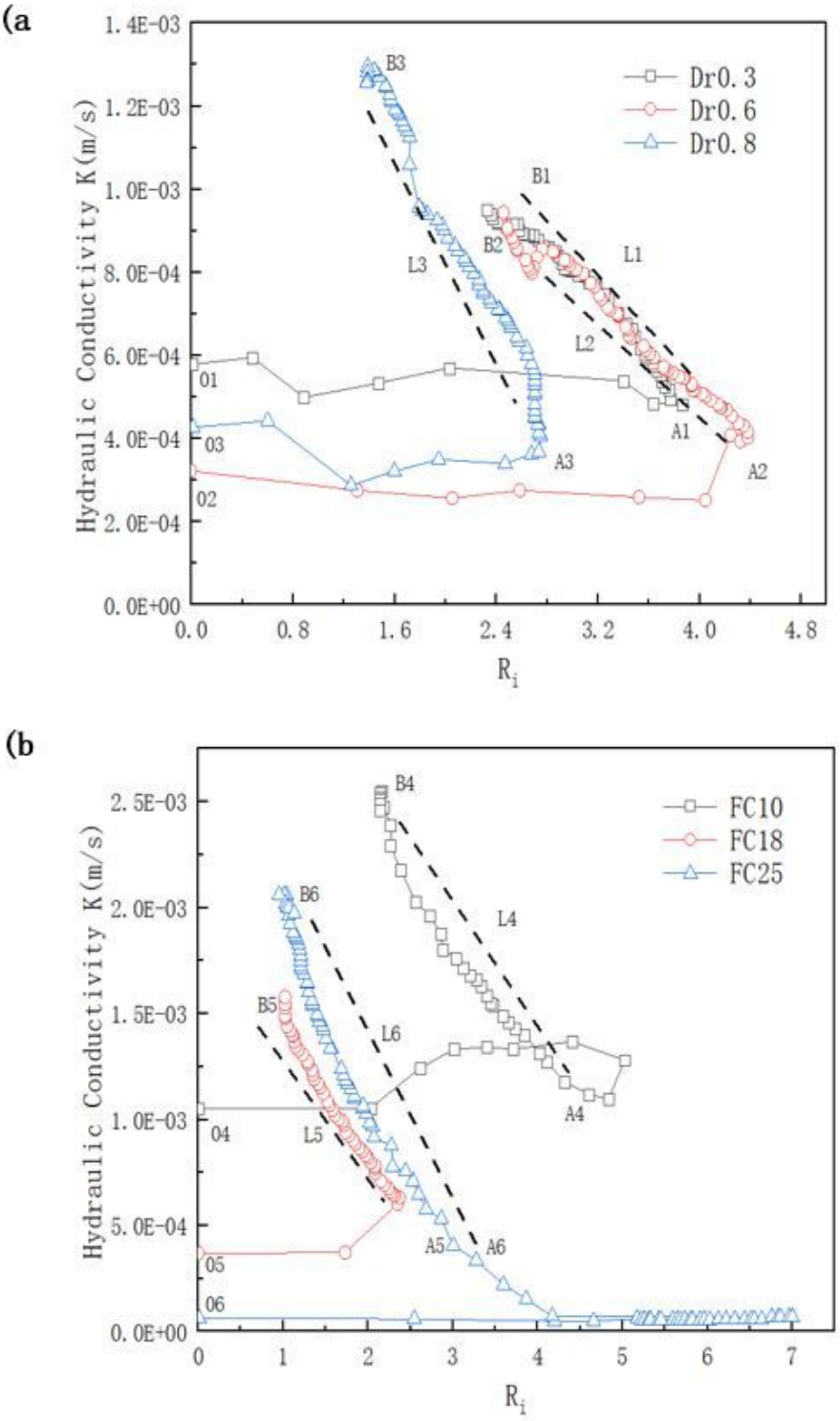

Figure 13

Variation in the hydraulic conductivity with Ri: (a) Dr group and (b) FC group.

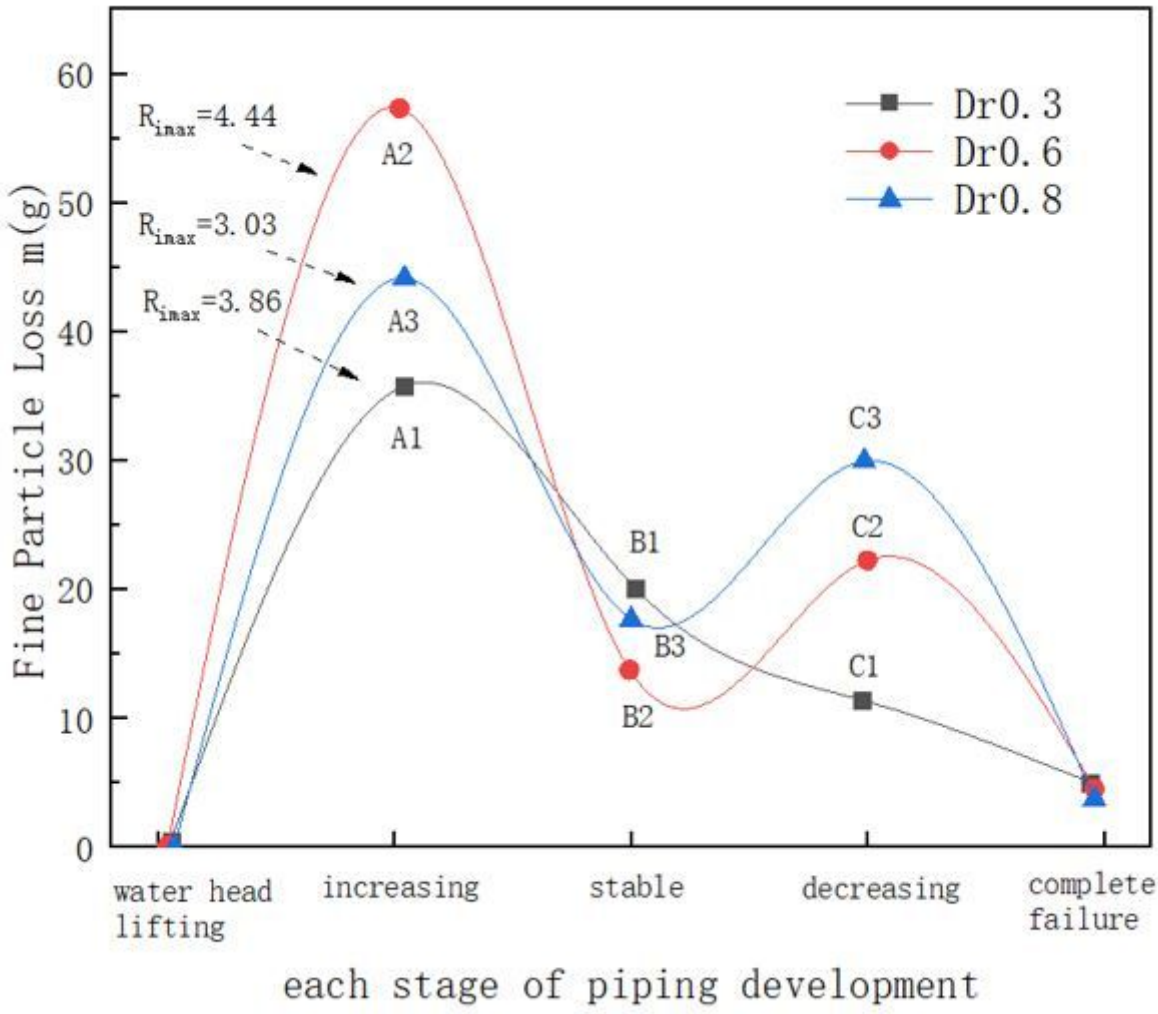

Figure 14

Loss of fine particles in different stages of piping erosion

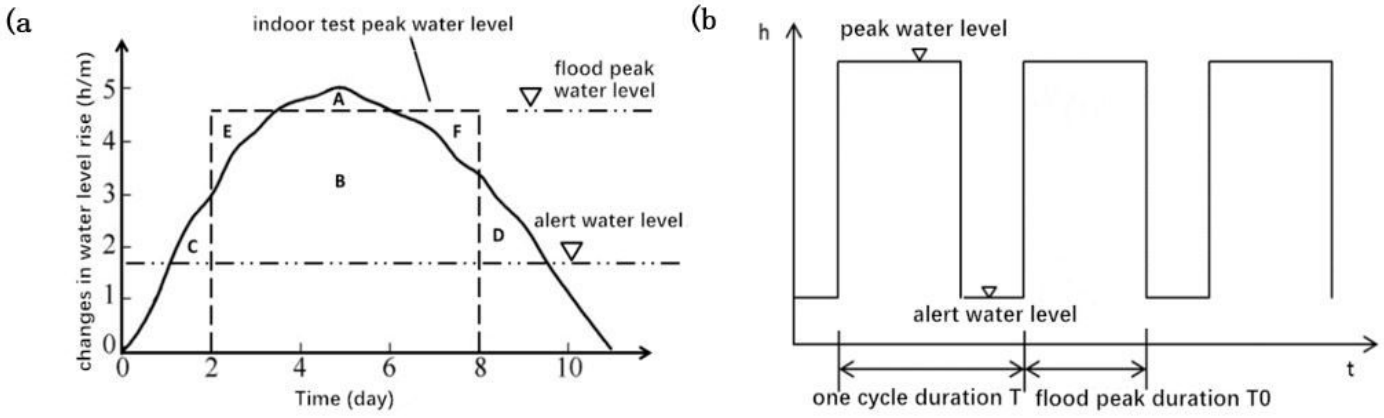

Figure 15

Flood peak process line: (a)Real flood peak process line and (b) Simplified flood peak process line.

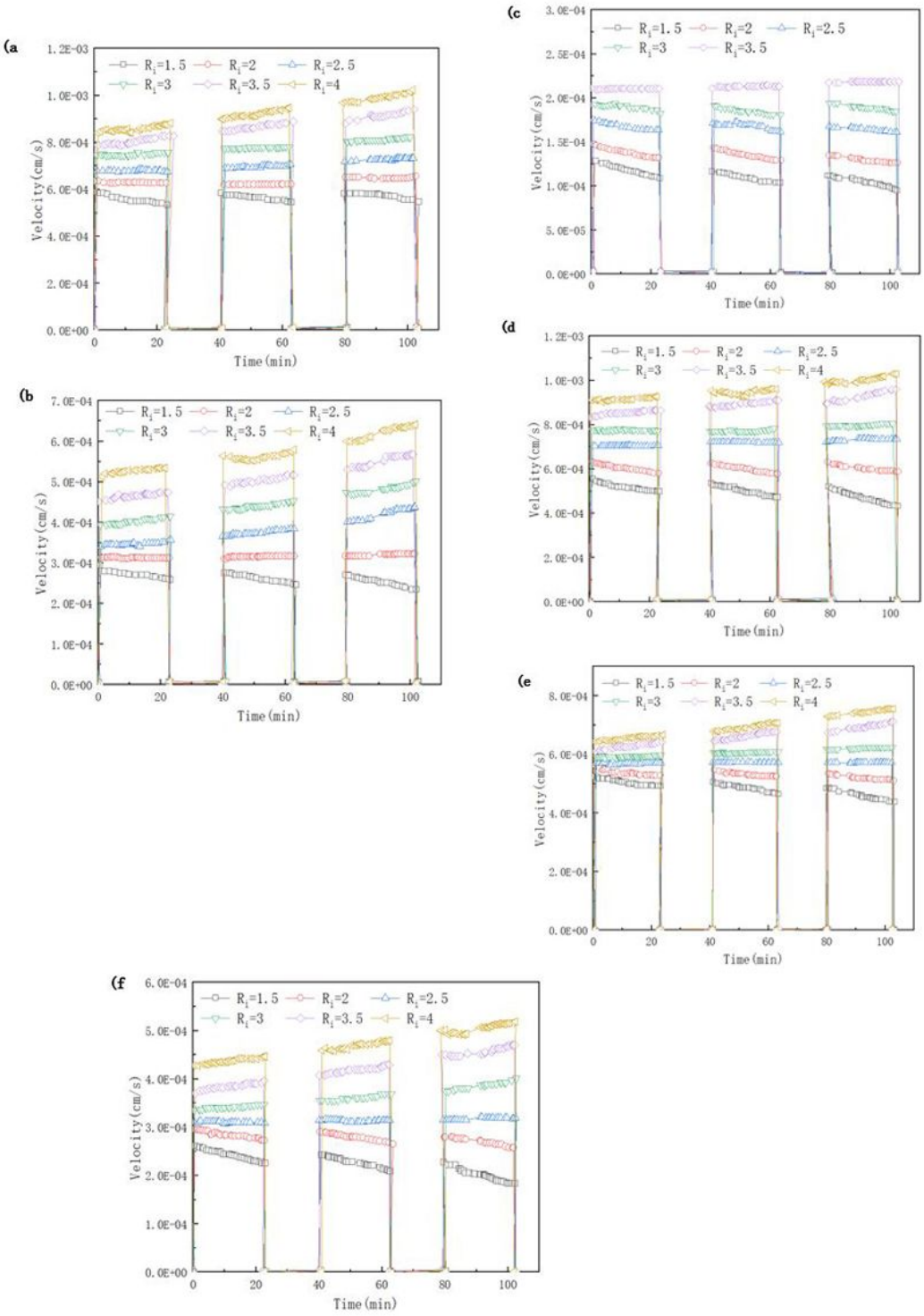

Figure 16

Variation in the flow velocity with time: (a) FC10 group; (b) FC18 group; (c) FC25 group; (d) Dr0.3; (e) Dr0.6; (f) Dr0.8.

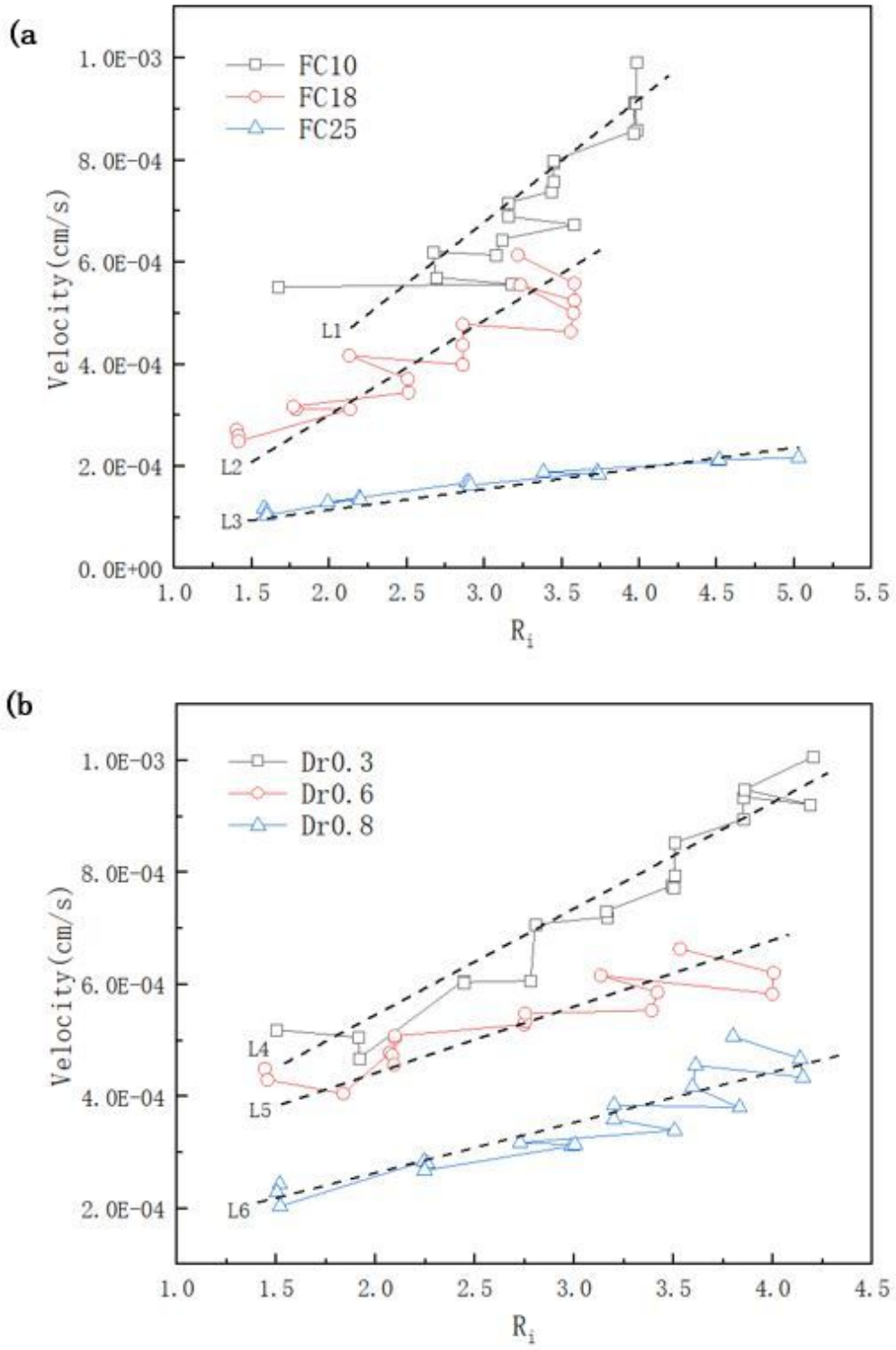

Figure 17

Variation in the velocity with Ri: (a) FC group and (b) Dr group.

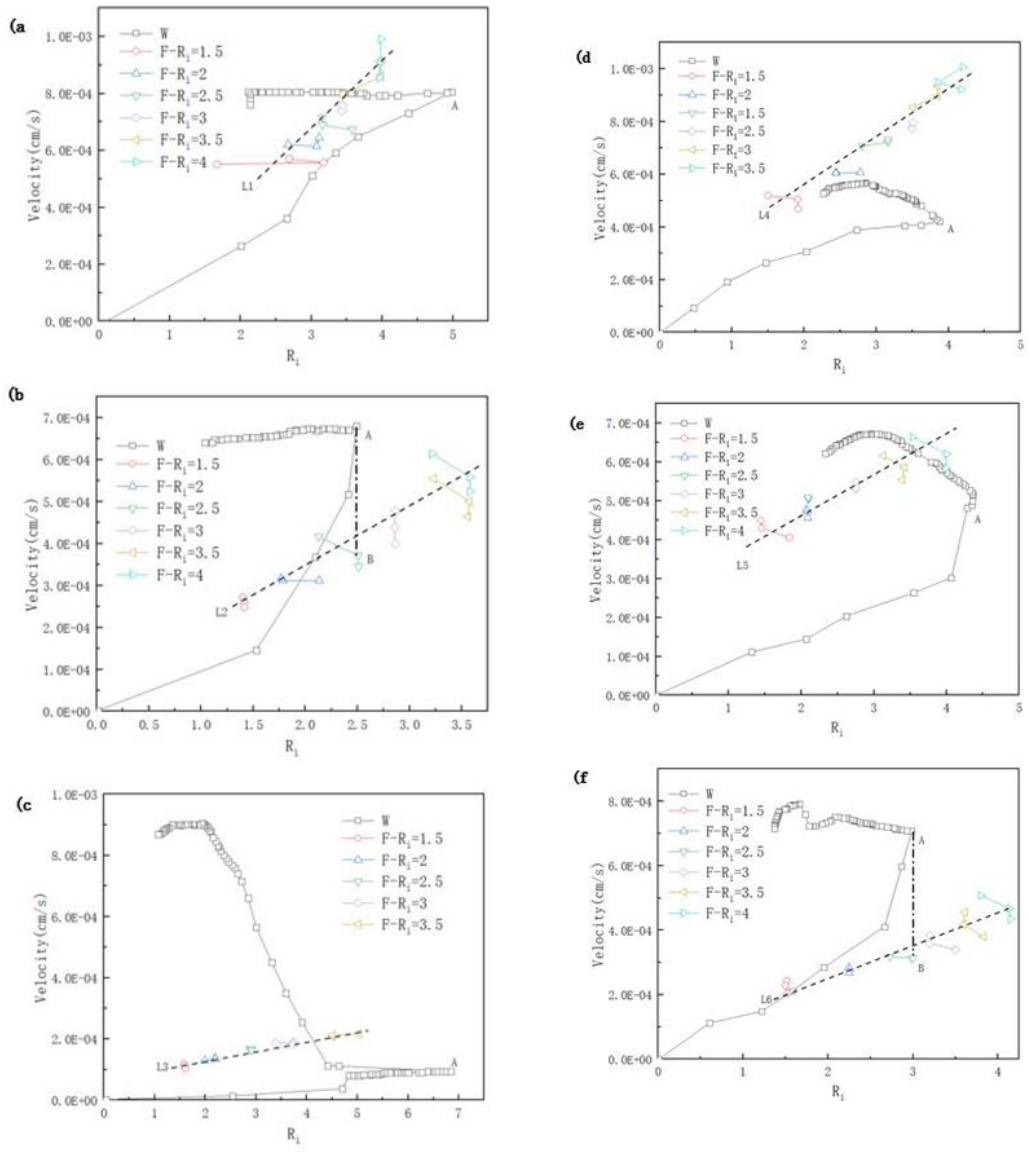

Figure 18

Comparison of the variation in the flow velocity with Ri: (a) FC10 group; (b) FC18 group; (c) FC25 group; (d) Dr0.3 group; (e) Dr0.6 group; (f) Dr0.8 group.